THE ROLE OF MICROTUBULES IN ATRIAL MECHANO-ARRHYTHMOGENESIS

By

Michael S. Connolly

Submitted in partial fulfilment of the requirements
for the degree of Master of Science

at

Dalhousie University
Halifax, Nova Scotia
July, 2022

Table of Contents

List of tables

List of figures

Abstract

In the heart, electrical excitation causes mechanical contraction, while feedback of the heart's mechanical state alters its electrical activity. With mechanical overload, this feedback can result in mechano-arrhythmogenesis (MA). In the ventricles, MA is driven by microtubule (MT) density/detyrosination in a transient receptor potential ankyrin 1 channel (TRPA1) dependent manner. Clinical evidence in the atria indicates arrhythmias are associated with increased TRP channels and pressure overload with MT densification.

My thesis aimed to determine if atrial MA is increased by MT density/detyrosination in a TRPA1-dependent manner.

This goal was unsuccessfully investigated using a chunk digested rabbit isolated atrial myocyte model. Modification of mechanical disruption, digestion time, enzyme concentration, calcium chelator exposure and calcium reintroduction were all shown to play a role in myocyte isolation. Unfortunately, extensive optimization did not reliably yield contractile myocytes.

This goal was successfully investigated using a Langendorff-digested rabbit isolated atrial myocyte model that underwent transient stretch with carbon fibres (CF). MA incidence was assessed after pharmacologic MT stabilization, which promoted MT density and detyrosination with paclitaxel, detyrosination inhibition with parthenolide or selective antagonism of TRPA1 with HC-030031. Acute stretch characteristics were determined during pharmacologic manipulations. Contractile properties (rate and amount of contraction) were evaluated with sarcomere tracking. MT density and/or detyrosination were measured in right atrial samples from cardiac surgery patients with normal or elevated right ventricle systolic pressures by western blot.

Here we found that increasing MT density and/or detyrosination with paclitaxel increases MA-incidence above a threshold level of stretch ($p=0.0183$). Co-incubation of paclitaxel with parthenolide or HC-030031 mitigates the increase in MA ($p>0.999$ and $p=0.5640$, respectively). Increased CF applied stretch increases the mechanical load per cross-sectional area, or cell stress. Myocyte contractile properties were improved by parthenolide. Patient pathologies may increase MT density and/or detyrosination.

Our results demonstrate that MT density and/or detyrosination may play a critical role in atrial MA through activation of mechano-sensitive TRPA1. Parthenolide inhibiting detyrosination may decrease cytoskeletal linkages in atrial myocytes, thereby improving contraction. Future work will determine if pressure overload in patients is associated with MT density and/or detyrosination and leads to an increase in atrial MA.

List of abbreviations

BDM	2,3-Butadione monoxime
BSA	Bovine Serum Albumin
CF	Carbon Fibre
CSA	Cell Surface Area
DGN	Digestion Solution
EGTA	Ethylene glycol-bis(β-aminoethyl ether)-N,N,N′,N′-tetraacetic acid
HC	HC-030031
IC_{50}	Inhibitory Concentration 50%
IHC	Immunohistochemistry
I/R	Ischemic reperfusion
KH	Krebs-Henseleit
LA	Left Atria
LAV	Left Atrial Volume
LV	Left Ventricle
LVEDD	Left Ventricular End Diastolic Diameter
LVEF	LV Ejection Fraction
LVESD	Left Ventricular End Systolic Diameter
MT	Microtubule
NaN	Not a Number
NCX	Sodium/calcium exchanger
NT	Normal Tyrode's Solution
PTL	Parthenolide
PZT	Piezo-electric translators
RAA	Right Atrial Appendage
REB	Research Ethics Board
RVSP	Right Ventricular Systolic Pressure
SAC	Stretch Activated Channel
SAC_{K+}	Potassium selective SAC
SAC_{NS}	Cation non-specific SAC
TAX	Paclitaxel
TCP	Tubulin Carboxypeptidase
TRP	Transient Receptor Potential channel
TRPA1	TRP ankyrin-1
TTL	Tubulin Tyrosine Ligase

Acknowledgements

To my family Steve, Heather, Erin, and Laura, thank you for always being there for me. To the Connolly and VanWart sides of the family, thank you for all you have done.

To Hannah, thank you for being so caring and patient; for supporting me through so many experiments. I always appreciate you looking out for me. You are amazing and I am excited for our next adventure.

To Matt, Enaam, Jon, Jessi, Ahmed, Katherine, and Zach you all contribute to making the Quinn lab productive, supportive and memorable. I will miss sitting around the conference table, snacking and drinking with you all.

To my COVID cohort of graduate students, Ahmed, Erica and Kirishani, this was a very strange time for graduate school and your company was among the best parts of this experience.

To the cardiac surgeons Dr. Edgar Chedrawy, Dr. Christine Herman and Dr. Greg Hirsch thank you for your time and the opportunity to work with patients. Additionally thank you to Gillian, Holly and Celeste for your assistance in consenting and collecting patient tissue.

To my committee members Dr. John Sapp, Dr. Keith Brunt, Dr. Ketul Chaudhary, and Dr. Yassine El Hiani for your supervision guidance and mentorship over the last 2 years. Additionally, thank you to both Keith and John for your mentorship, training, and supervision over last 5 and 2 years. You all have greatly shaped my academic and professional careers and helped me become a better researcher.

Carbon Fibres used in these experiments were gift from Jean-Yves LeGuennec and supplied by Prof. Peter Kohl, Institute for Experimental Cardiovascular Medicine, University Heart Centre Freiburg / Bad Krozingen. ImageJ program to calculate microtubule density per unit area provided by Dr. Matthew Caporizzo and Dr. Benjamin Prosser, Department of Physiology, University of Pennsylvania Perelman School of Medicine, Philadelphia, USA.

I had the assistance of an undergraduate Medical Sciences student, Emma Delong, who performed the cell staining, imaging, and density quantification to produce microtubule density results. Many thanks to Dr. Bre Cameron for technical assistance and training with the carbon fibre method. Thank you to Dr. Lester Perez and Ashley Eadie for training in protein isolation and western blotting. Thank you to Joachim Greiner and Dr. Rémi Peyronnet for consultation on human cell isolations. Many thanks to the most important piece of lab equipment, the coffee machine, for always working and keeping the lab functioning.

Most importantly thank you to Dr. Alex Quinn for your unwavering support and excellent counsel. I admire your tireless work ethic and problem-solving ability which I hope to live up to. Your dedication to your trainees is exceptional and I would not have been able to complete this degree without your help. Your contributions to the lab and to my development as a student, researcher, writer and person cannot go understated, thank you again.

Chapter 1. Introduction

1.1 Mechano-electric coupling

The heart supplies the body with oxygen and nutrients by precisely coordinating billions of individual cells. The heart beats approximately once per second and ~3–4 billion times in one's lifetime [1]. The heart is comprised of individual muscle cells (cardiomyocytes) that are electrically excited and mechanically contract in a well-coordinated pattern that adjusts on a beat-by-beat basis to match the haemodynamic demand of the body. That systemic demand in the body can change due to postural or circadian oscillations, exercise, or autonomic changes. To match changes in demand, the heart has a system of feed-forward (excitation-contraction coupling) and feed-back (mechano-electric coupling) loops. Briefly, excitation-contraction coupling is where the leading pacemaker in the sinoatrial node (SAN) causes a wave of depolarization, causing calcium entry into the cardiomyocyte through voltage-gated channels, calcium-induced calcium release from the sarcoplasmic reticulum then, free calcium binds troponin C to initiate cross-bridge cycling[2,3].

The Mechano-Electric Coupling (MEC) feedback system encompasses all mechanical stimuli acting on the heart irrespective of origin [1,4]. When acute cardiac mechanical activity acts as an input signal, it is known as "mechano-elektrische Rückkopplung" in German (in English Mechano-Electric Feedback; MEF)[5,6]. Mechanical stimuli, such as membrane tension, directly act on Stretch Activated Channels (SAC) to cause a response within milliseconds[1,7]. Stretch modulated ion channels have their activity altered (and usually increased) in response to mechanical stimuli. Mechanical stimuli changes calcium handling and secondary messenger systems to effect excitability, refractoriness, electrical load, heart rate and rhythm, and conductance [1,8–10]. Cardiovascular disease alters MEC in the heart with important clinical consequences. Pathophysiologic changes in mechano-sensitivity, myocardial mechanics, or the mechanical environment may contribute to mechanically induced alterations in cardiac electrophysiology that result in arrhythmogenesis, or ectopic contractions, known as Mechano-Arrhythmogenesis (MA)[11]. These processes form the Mechano-Electric Regulatory Loop (Figure 1). The mechano-sensitivity that defines MEC is driven by components that transduce stimulus (Mechano-Electric Transducers)[12], that effect the electrical response (Mechano-Electric Effectors)[7], and those that mediate responses (Mechano-Electric mediators)[13].

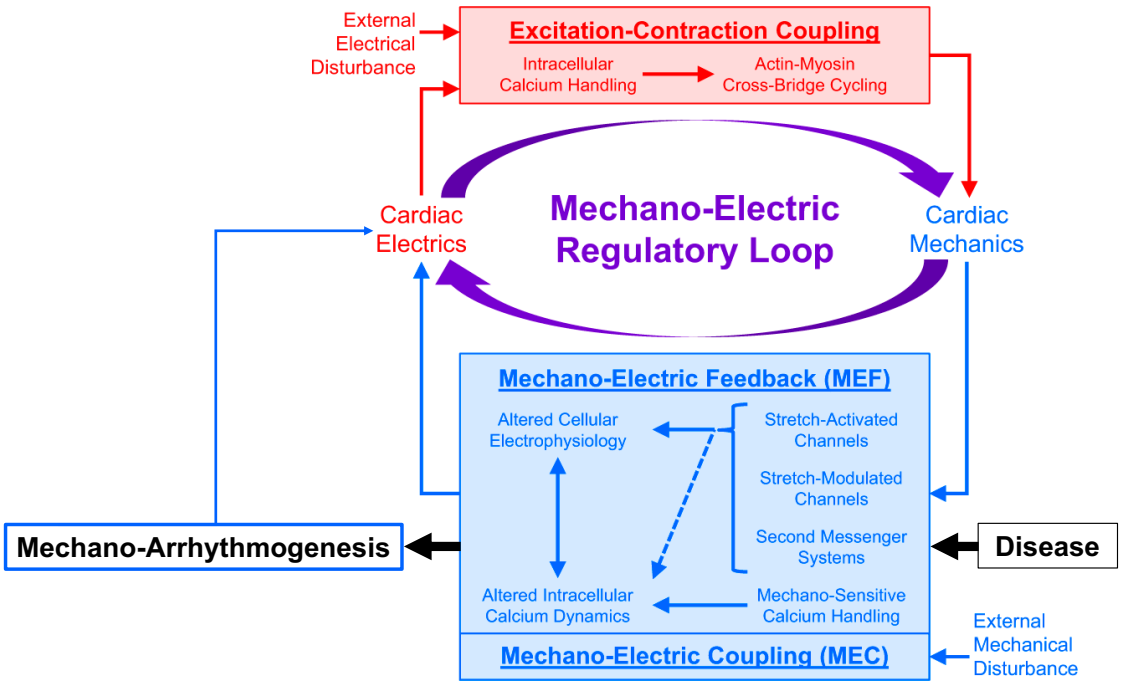

Figure 1. Intracardiac mechano-electric regulatory loop. The feed-forward and feedback links between cardiac electrophysiology and cardiac mechanics compose the mechano-electric regulatory loop. Excitation-contraction coupling is the feed-forward loop where electrically excited calcium release causes mechanical contraction through actin-myosin cross-bridge cycling. Cell deformation is detected by interdependent mechanosensitive mechanisms act as the feedback loop. Mechanosensitive feedback alters cellular electrophysiology and intracellular calcium, therefore effecting the origin and spread of excitation, known as Mechano Electric Feedback. Disease may alter mechanosensitive mechanisms. External mechanical stimuli that alters cardiac electrical activity is more broadly known as Mechano Electric Coupling. Mechanical stimuli that result in arrhythmogenesis is known as Mechano-Arrhythmogenesis. Adapted from[1].

1.1.1 Mechano-electric transducers

Mechano-electric transducers sense mechanical stimuli and transmit those stimuli to mechano-electric effectors and mediators to elicit or modulate electrophysiological responses[14,15]. In cardiomyocytes, microtubules (MT) play a key role in mechano-electric transduction, especially during stretch, alongside other cytoskeletal elements like titin, microfilaments, desmins and integrins [12,16,17]. MT are the stiffest cytoskeletal filaments that provide cellular structural support, interact with membrane-associated proteins and intermediate proteins, and can transduce mechanical signals to other mechanosensitive subcellular components [14,18].

MT are dynamic and undergo rounds of growth (polymerization of αβ-tubulin through GTP hydrolysis) and shrinkage (catastrophe; loss of GTP-tubulin cap and sudden, rapidly shortening of an MT) [19]. Increasing MT stability means that MTs remain as fixed structures from minutes to hours. Further stabilization of MTs is provided by structural MT-associated proteins and post-translational modifications such as detyrosination/tyrosination, phosphorylation, glutamylation, glycosylation, acetylation/deacetylation, polyamination, and palmitoylation[20].

MT stabilization determines sarcomere stiffness and stability. The amount of tyrosination is inversely proportional to the viscoelastic stiffness of the sarcomere. Sarcomeric anchors are formed by detyrosinated MT interacting with desmin, stabilizing the MT and providing resistance to contraction. Detyrosination status determines load-bearing ability of the cardiomyocyte. As such, the more detyrosinated the MT—the more stable and resistant the sarcomere is to mechanical load during contraction. Inhibiting detyrosination increases allows unanchored MT to slide past each other during contraction of the sarcomere[21].

The tyrosination cycle regulates MT detyrosination and stability. Tubulin carboxypeptidases (TCP) reversibly remove C-terminal tyrosine of α-tubulin from polymerized MT (detyrosinated MT). The addition of tyrosine residues to soluble tubulin is performed by Tubulin Tyrosine Ligase (TTL)[22,23]. Detyrosinated MT is more stable because they resist sudden rapid disassembly of MT into tubulin heterodimers (catastrophe)[22]. Parthenolide (PTL) can inhibit TCP and therefore inhibit the detyrosination of MT and decrease myocyte stiffness [24]. In contrast to PTL, paclitaxel (TAX) stabilizes MTs and increases the proportion of detyrosinated MT[21].

Increasing MT stability, in turn, increases stiffness. How myocytes react to passive mechanical stretch of cells before contraction is "strain" (when normalized to

resting length) and the load against which cells actively contract is "stress" (when expressed as force per cross-sectional area)[1,25]. The relationship between stress and strain describes the elastance of the cell. Myocytes exhibit non-linear viscoelasticity, meaning that stress and strain properties will differ depending on the amount and rate of stretch applied. MT alter non-linear viscoelastic properties in myocytes as MT contribute to cardiomyocyte stress only at fast rates of stretch [25,26]. Taken together these factors increase mechano-electric transduction during acute mechanical stimuli.

1.1.2 Mechano-electric effectors

Mechano-electric effectors cause an electrical change in response to mechanical stimuli [7]. SAC have currents that are gated or augmented by stretch can lead to depolarization or altered repolarization of the membrane potential. The balance of the two currents determines whether the membrane potential will depolarize or repolarize. Potassium selective SAC (SAC_{K+}) mainly contributes to the repolarization of a healthy cardiomyocyte, and it has been reported that SAC_{K+} does not dominate the overall MEC response compared to Cation non-specific SAC (SAC_{NS})[1,27].

SAC_{NS} can lead to depolarization or altered repolarization depending on the timing of the stretch. Therefore, it is suspected that SAC_{NS} may have a reversal potential of ~0 mV, and the timing of mechanical stimuli determines if the channel passes an inward depolarizing current or outward repolarizing current[1,28]. If a mechanical stimulus was applied in diastole and the depolarizing current was supra-threshold, then an ectopic stretch-induced excitation would occur[29]. There remains a lack of consensus if mechano-electric effectors are driven by stretch, stretch-rate, or tension. While the effects of SAC_{NS} are well characterized, it has yet to be assessed by single-channel recordings.

One suspect for the identity of cardiac SAC_{NS} are Transient Receptor Potential (TRP) channel family with six subfamilies[30,31]. These channels have been shown to be mechanosensitive and pass inward or outward currents[32,33]. Broadly, the TRP family of channels are associated with (possibly linked to) the cytoskeleton[34]. Specifically, TRP Ankyrin 1 (TRPA1) channels have been implicated in cardiovascular diseases, such as atherosclerosis, myocardial fibrosis, heart failure, and arrhythmia[30].

1.1.3 Mechano-electric mediators

Mechano-Electric Mediators are present in the heart. They modulate the intracellular electrophysiologic response to a mechanical stimulus [13,35]. They function during the stretch-induced release of intracellular calcium[18] and reactive oxidative

species,[36] which can further enhance mechano-transduction. Mechano-electric mediators can also contribute to MEC.

1.2 Mechano-arrhythmogenesis

Mechanical stimuli occur with enough stimulus to be conducted via mechano-electric transducers and act on mechano-electric effectors to elicit supra-threshold depolarization resulting in MA at the correct time. Pathophysiology substrates altering the mechano-electric transducers and effectors can subsequently alter mechano-sensitivity to increase the probability of overcoming the temporally dependent magnitude-threshold that triggers arrhythmia[1,37].

1.2.1 Clinical evidence for mechano- arrhythmogenesis

Commotio cordis is the most striking example of MA, where non-penetrating mechanical impact of the pre-cordial chest—absent of any microscopic damage—causes serious dysrhythmia and risk of sudden cardiac death [38]. MA is more commonly seen in the ventricle during procedures involving central vascular or intracardiac catheters, electrodes, and balloon valvuloplasty that cause local tissue deformation and lead to ectopic contractions and arrhythmia [39–42]. The risk of MA is increased further during cardiovascular diseases (such as: valve disease, cardiomyopathy, heart failure, hypertrophy, ischemia, or infarction) where acute changes in ventricular pressure or volume are more likely to result in premature excitation and arrhythmia [6,43].

1.2.2 Pressure-overload in the atria

The atria's ability to acutely respond to stretch was first described 100 years ago by Bainbridge, wherein acute distension of the right atria by increased venous filling pressure accelerated heart-rate in dogs[5,44]. Pressure-overload promotes alterations in mechano-electric transducers that increase susceptibility to MA. Increased haemodynamic load in the atria—as with hypertension, heart failure, or mitral valve disease—increase the stretch of tissue and are associated with increased arrhythmia [45]. MT stabilization and increased density are characteristics of right ventricular pressure-overload [46] and we believe this contributes to altered contractile properties as seen in the ventricle[47]. MTs may be further implicated in atrial mechano-transduction because some double-blind randomized control trials show that decreasing MT stability with colchicine reduces postoperative atrial fibrillation [48].

1.3 Atrial mechano-arrhythmogenesis

Pressure-overload in the left atria is associated with increased calcium leak from the sarcoplasmic reticulum and atrial fibrillation [49]. Acute stretch promotes atrial

refractoriness and the potential for triggering premature beats and atrial fibrillation [50]. In settings of atrial pressure overload, with the associated increase in MT density, the reduced magnitude of an acute mechanical stimulus needed for ectopy could contribute to mechanically triggered arrhythmia.

A potential driver for MA in the atria is TRPA1 acting as a mechano-electric effector. TRPA1 has been shown to drive both systolic and diastolic MA in the ventricle in a stretch dependant manner. Ventricular mechanosensitivity was shown to be altered through modulation of MTs[11]. TRPA1 was suggested to be in the atria, though it remains unknown as a contributor to atrial MA[33,51]. While mechanisms of MEC-induced arrhythmias have been described with emerging evidence as to the importance of MT and TRPA1 for MA in the ventricles, what role they have in the atria is unknown.

1.4 Objective, hypothesis, and aims

Based on this gap in our knowledge of atrial MA, the **objective** of my thesis research was to determine the importance of MTs and TRPA1 in atrial MA. I **hypothesized** that much like in ventricular myocytes, an increase in MT density and/or detyrosination in atrial myocytes would increase MA in a TRPA1-dependent manner. This hypothesis was addressed through two Aims:

Aim 1: Explore factors contributing to atrial MA by the controlled stretch of rabbit isolated atrial myocytes with pharmacologic manipulation of MT or TRPA1.

Aim 2: Translate cardiomyocyte isolation and single cardiomyocyte stretch approach to human atrial samples acquired from patients with and without right-sided pressure overload undergoing cardiac surgery.

Chapter 2. Atrial myocyte isolation

2.1 General methodological considerations

Isolated cardiac myocytes have been fundamental to investigating mechanistic pathways, understanding physiology and pathology, and developing new therapeutic approaches [52]. For mechano-electric coupling investigations, the benefit of working with isolated cardiomyocytes is the precise control of the mechanical environment and fluorescent visualization of subcellular components with minimized whole tissue variability. Early work in cardiomyocyte isolation involved removing ventricular tissue from rats to be submerged in an enzyme-containing solution thus freeing single cardiomyocytes, a process referred to as: the 'chunk' digestion method [53].

Chunk digestion of animal cardiac tissue was later supplemented with a whole heart isolation method. In that protocol, the heart is rapidly isolated and the aorta sutured to a cannula which is attached to a Langendorff apparatus so that the heart undergoes retrograde perfusion. Blends of enzymes are added to the perfusate to break down the extracellular matrix. The degraded tissue is subsequently mechanically dissociated into individual cells. This method will be referred to as the 'Langendorff perfusion' method [54]. Early work in rabbits using the Langendorff perfusion method was adapted from earlier murine protocols[55].

The majority of modern small mammal cardiomyocyte isolation techniques now use isolated heart Langendorff perfusion to maximize cardiomyocyte viability and reproducibility [56–58]. Larger mammals and explanted human hearts may also have the aorta cannulated or, due to experiential constraints and sample availability, the circumflex or right coronary arteries may be directly perfused [59,60]. Recent modifications to both small mammal, large mammal, and human cardiomyocyte isolation protocols include vibratome slicing of tissue, which undergoes further digestion to improve overall cardiomyocyte viability [52,61]. In most methods, the isolation of healthy single cardiomyocytes is achieved by the same broad mechanisms, but underlying techniques vary between research groups with no definitive or standardized method.

2.1.1 Calcium paradox

The calcium paradox is a technical artifact of isolated single cardiomyocytes whereby reintroduction of extracellular calcium necessary for viability also risks irreversible hypercontraction or infolding from their native cuboidal/rectangular shape[62,63]. It was discovered by accident in 1966 [64]as the irreversible contraction of myocytes, cessation of all electrical activity, and cardiomyocyte death upon the

reintroduction of calcium and has since plagued investigations of isolated cardiomyocytes. Protecting myocytes from the deleterious effects of the calcium paradox increases the number, survival, and viability of isolated cardiomyocytes and is thus foundational to cardioplegic solutions, cardiomyocyte isolations, and investigation into ischemic reperfusion injury (I/R) [64,65].

The purpose of a calcium-free period in cardiac myocyte isolation is to disrupt the intracellular junctions between cardiomyocytes through the interruption of calcium dependant cadherins. Functionally, an incubation with calcium-free solution improves isolated cardiomyocyte yield [61,66,67]. There are two main hypotheses for the mechanisms of cellular injury occurring due to the reintroduction of calcium to the cardiomyocyte. The first hypothesis posits that cardiomyocyte-cardiomyocyte attachments are weakened during calcium-free incubation, and, upon the return of calcium, sarcomere contraction perforates the sarcolemma. Heterogenous uncoupling of excitation and contraction on a tissue level creates sites for acute excesses of mechanical tension, which can damage the sarcolemma. The mechanical damage is the cause of secondary functional and structural changes, such as a secondary influx of calcium causing terminal hypercontraction, mitochondrial damage, and myoglobin release [62,68]. A limitation of this proposed hypothesis for the calcium paradox is that key cardiomyocyte-cardiomyocyte interactions that cause sarcolemma damage are not present in isolated cardiomyocytes, where the calcium paradox still exists [63,69].

More recent work supports an alternative hypothesis, that the calcium-free period increases the permeabilization of the sarcolemma to electrolytes and water, resulting in damage. Specifically, if both calcium and magnesium are depleted, then intracellular sodium concentration can increase by sodium conductance *via* L-type calcium channels and inhibition of sodium/potassium ATPase (Na+/K+ ATPase) occurs by reperfusion injury [70–72]. Upon calcium reintroduction, Na+/K+ ATPase remains impaired and excessive calcium uptake occurs secondary to sodium overload *via* the reverse mode of the sodium/calcium exchanger (NCX), resulting in hypercontraction [70,71,73]. The ensuing increase in intracellular cation concentration and sarcolemma disruption may also contribute to osmotic swelling. Omachi *et al*. have reported that calcium-free solution made either isotonic or hypertonic with an addition of 150-200 mM of sucrose was protective against the calcium paradox by preventing cardiomyocyte swelling [74]. However, that study may be confounded because of the concurrent reduction of sodium to maintain isotonicity in the experimental condition.

Commonly, cardiomyocyte isolation protocols include Bovine Serum Albumin (BSA) to increase the oncotic pressure [52,59]. Digestion solutions can be supplemented with 2,3-Butanedione Monoxime (BDM), a chemical phosphatase inhibiting cross-bridge cycling, uncoupling cardiac contraction. Supplementation with BDM (subsequently increasing solution osmolarity, discussed above) has been protective during tissue cutting and during calcium reintroduction [68,75,76]. Other common use reagents shown to improve cardiomyocyte health during cardiomyocyte isolation include Krebs cycle intermediaries, taurine, and creatine to increase intracellular ATP[59,77,78].

2.2 Chunk digestion method

Aim 2 of our research objectives involved the use of cardiomyocytes isolated from human atrial tissue samples collected from patients during cardiac surgery. As this would require a chunk digestion method, we initially sought to establish this technique using pieces of rabbit atria from isolated hearts. Secondary benefits of isolating rabbit cardiomyocytes *via* chunk digestion were that cardiomyocytes would be acquired by a similar means in the two sets of experiments and that it would reduce the usage of animals as the cardiomyocyte isolation could be paired with ventricular experiments. To achieve this goal, substantial experimental optimization was required.

The following protocol was our final iteration on this method. Female New Zealand White rabbits (2.1 ± 0.2 kg, Charles River) were used as a small animal model due to their relevance for cardiac arrhythmia research [79–81]. Rabbits were euthanized by ear vein injection of pentobarbital (140 mg/kg) and heparin (375 units/kg, Sigma-Aldrich), followed by rapid excision of the heart, aortic cannulation, and Langendorff perfusion (20 mL/min) with 37°C Krebs-Henseleit (KH) solution, containing (in mM): 132 NaCl, 4.7 KCl, 21 $NaHCO_3$, 1.4 NaH_2PO_4, 10 glucose, 1 $MgCl_2$, 1.8 $CaCl_2$, (Sigma-Aldrich), with an osmolality of 300 ± 5 mOsm/L and bubbled with carbogen (95% oxygen / 5% carbon dioxide) to a pH of 7.40 ± 0.03. After a rest period of 15 min, a portion of the left atria was removed with scissors.

To digest the atria chunk, it was transferred to a custom two-chamber enzymatic digestion bath that was water jacketed to maintain 37°C and bubbled with 100% oxygen at a rate to keep the tissue from remaining settled at the bottom. The tissue chunk was immersed for 5 minutes in the first chamber containing a calcium-free Wash Solution, containing (in mM): 142 NaCl, 5 KH_2PO_4, 1 $MgSO_4(7H_2O)$, 10 glucose, 10 HEPES, 9.5 Taurine, 0.1% w/v Albumin, 0.2 EGTA (Sigma-Aldrich), with pH adjusted to 7.40 ± 0.03 with NaOH and an osmolality of 300 ± 5 mOsm/L. The tissue chunk was then moved to

the second chamber containing the Digestion Solution, composed of (in mM): 142 NaCl, 5 KH_2PO_4, 1 $MgSO_4(7H_2O)$, 10 glucose, 10 HEPES, 9.5 Taurine, 0.02 $CaCl_2$, 0.1% w/v Albumin (Sigma-Aldrich), along with 200 U/mL Collagenase II (Worthington Biochemical Corporation) and 0.54 U/mL Protease XIV (from Streptomyces griseus, Sigma Aldrich), with pH adjusted to 7.40 ± 0.03 with NaOH and an osmolality of 300 ± 5 mOsm/L for 20 minutes. The tissue chunk was further digested for 10 minutes in collagenase-only containing Digestion solution. Enzymatic digestion was stopped by placing the tissue chunk in Kraft-Brühe solution (KB; German for 'power-soup'), containing (in mM): 20 KCl, 10 KH_2PO_4, 25 Glucose, 40 D-Mannitol, 70 K-Glutamate, 10 β-Hydroxybutyrate, 20 Taurine, 10 EGTA, 0.1% w/v Albumin (Sigma-Aldrich), with pH adjusted to 7.40 ± 0.03 with KOH and an osmolality of 300 ± 5 mOsm/L) [82,83].

Cardiomyocytes were freed from the tissue chunk *via* mechanical disruption using a 10 mL pipette tip cut to have a 1 cm opening to triturate the tissue chunks in KB solution for 7.5 minutes. The cardiomyocyte-containing solution was filtered through a mesh with 250 μm openings to remove undigested pieces of tissue, collagen, and fat. The filtered solution was aliquoted into 2 mL Eppendorf tubes and stored at 4°C for up to 6 hours. The remaining piece of tissue was subsequently moved to new KB solution, cut into 1 mm^3 pieces and pulled apart with forceps to free cardiomyocytes. This cardiomyocyte containing solution was also filtered, aliquoted, and stored at 4°C.

Calcium was reintroduced to the solution at room temperature prior to experimentation. Cardiomyocytes aliquoted in 1 mL of KB solution were removed from the fridge and left to settle by gravity in 2 mL Eppendorf tubes for 10 minutes. The supernatant was removed and 10% of the solution was replaced with Normal Tyrode's solution (NT), containing (in mM): 142 NaCl, 4.7 KCl, 1 $MgCl_2$, 1.8 $CaCl_2$, 10 glucose, 10 HEPES (Sigma-Aldrich), with a pH adjusted to 7.40 ± 0.03 with NaOH and an osmolality of 300 ± 5 mOsm/L. At subsequent 10-minute intervals, 20%, 50% and 100% of the supernatant was removed and replaced with NT.

2.3 Chunk digestion optimization

Isolating cardiomyocytes is challenging even for experienced operators with batch-to-batch variability between experiments [56,84,85]. Experimental variability in cardiomyocyte isolation often arises from improper handling, variable water quality, improper albumin concentration, or enzyme quality [86], concentration, and blend often being the most likely variables[87]. Due to the initial lack of calcium tolerance and no contractile function of our early cardiomyocyte isolations, we attempted to optimize our

protocol. Digestion solution volume was maintained so that cardiomyocyte concentrations were comparable between experiments. Cardiomyocyte counts were averaged between aliquots.

Table 1 summarises the variables considered for optimization, the rationale for doing so, how they were manipulated, and the outcome in our attempts to improve our viable cardiomyocyte yield (green = improvement, gray = no change, red = worse).

Table 1: Manipulated variables to optimize chunk digestion

	Variable	Rationale	Manipulation	Outcome	Reference
1	Tissue disruption method	Pulling apart tissue with forceps may be damaging cardiomyocytes	Trituration of digested chunks with a custom large diameter pipette tip	Improves disruption in small volumes or tissue sizes	59,83,86–88
2	Rest period	Incubation in a high K+ medium may normalize intracellular Na+/K+ ratios	Resting the cardiomyocytes after isolation in KB solution for 60 minutes	No change to the number of cardiomyocytes or response to pacing stimulus	82,89,90
3	Strain tissue through a mesh	Viable cardiomyocytes may be stuck to under digested tissue and cardiomyocyte sheets and thus lost during straining	Remove mesh	Mesh was key to limiting fat and collagen in the cardiomyocyte solution that impairs experimentation	86
4	Protease Concentration	Exposure to elevated levels of protease damage cardiomyocytes and I_{Kr} channels	Decrease protease by an order of magnitude	Cardiomyocyte membrane quality improved and were more straight, increased number of doublets	91
5	Protease Time	See above	Minimize exposure to protease-containing solution	Determined minimal threshold for protease exposure was 20 minutes	87,92
6	Collagenase time	Exposure to elevated levels of collagenase damage the sarcolemma	Minimize exposure to collagenase containing solution	Determined minimal threshold for collagenase exposure was 30 minutes	87
7	EGTA exposure	EGTA may be affecting	Removal of EGTA from all solutions	Cardiomyocyte isolation success dropped from 100% to 40%. Number of cardiomyocytes responding to pacing stimulus decrease by 50%	59,93,94

2.3.1 Mechanical disruption and tissue handling

It is important to minimize mechanical stress to the chunks of tissue when isolating cardiomyocytes [59,83,86]. Stretching tissue with forceps directly in the inverted microscope bath was helpful to myocyte release but contaminated the bath with undigested cellular matter, dead cells, and fat.

Various mechanical disruptions can be applied to the tissue to free cells. In our experience, when working with small amounts of tissue, using a trituration method is more efficient, consistent, and gentle compared to using forceps. While trituration can be applied with a cut-down transfer pipette, a 1 mL pipette, and a 2 mL stripette we had the best success using a 10 mL plastic pipette that was cut and heat treated so there was a large opening with no sharp edges. This pipette was set to 3mL and effectively disrupted tissue in 5 mL of stop solution to mitigate the bubbles produced by BSA. We found that under digestion or improper cardiomyocyte handling decreased the number of isolated cardiomyocytes. Straining the isolated solution was critical to removing debris and fat, which adhered to the mesh. Iterations completed across 10 experiments resulted in cardiomyocyte count in KB solution increasing from ~6 cardiomyocytes/ mL to ~100 cardiomyocytes/ mL.

2.3.2 Calcium reintroduction

The process of calcium reintroduction is a critical factor, and we found that more atrial cardiomyocytes would tolerate physiologic calcium concentration when the rate of reintroduction to 1.8 mM calcium decreased. Previous work showed that ventricular myocytes tolerated 50% calcium reintroduction steps every 10 minutes [95]. Attempts at a 50% calcium reintroduction decreased the number of cardiomyocytes in NT to ~1cardiomyocyte/mL (N=3). For atrial myocytes, decreasing the rate of calcium reintroduction to 10, 20, 50, and 100% NT replacements every 10 minutes improved cardiomyocyte viability. Cardiomyocytes were more calcium tolerant, responsive to pacing stimulus and quiescent in the absence of pacing stimulus. Decreasing the rate of calcium reintroduction further has diminishing returns, as a 9-step calcium reintroduction protocol did not have observable improvements to cardiomyocyte viability. Separately, the nominal calcium reintroduction occurring in the digestion solution required for enzyme function is unlikely to impair Na+/K+ ATPase activity if below 0.05 mM Ca^{2+} [71].

2.3.3 Enzymes

Digestive enzymes are critical to release cardiomyocytes from the extracellular matrix. Factors that alter digestive enzyme efficiency include concentration, tissue type,

dissociation medium, incubation time, and batch-to-batch variability. An issue common to digestion enzymes is that myocytes along with connective tissue can be degraded, or damage to ion channels can occur, which is worse during chunk digestion than with Langendorff perfusion. As seen in[91] I_k currents were only present in 4% of cardiomyocytes isolated via chunk method compared to 96% of cardiomyocytes isolated via perfusion method. For example, proteases like Type XIV and Type XXIV (Sigma) have been shown to selectively damage I_{kr} channels without lysing the cardiomyocyte[92,96].

To resolve having cardiomyocytes not contract in response to pacing stimuli, we altered digestion parameters. First, to mitigate calcium dependant activity of collagenase by intentionally delaying the addition of nominal calcium and promoting digestion by protease alone [87,97]. Then, adjusting protease mixtures that contain calcium acetate as a stabilizing agent, which ranges between 2-30% (w/w). The contribution of protease stabilizing agents to overall calcium concentration of the solution is often ignored. This small amount of calcium could allow for some activity of collagenase if the digestive enzymes were applied concurrently. In our hands, the calculated contribution of calcium may have been between ~0.5 μM to ~7.6 μM and was likely negligible. We also tried limiting protease exposure by removing the tissue chunks from the protease-containing solution and immersing chunks in a collagenase-only digestion solution.

Protease and collagenase exposures were decreased alternatingly. Initial experiments had enzyme exposure held constant. Comparing sequential experiments where protease concentration was dropped by an order of magnitude (5.4 U/ mL to 0.54 U/ mL). A doubling to 256 cardiomyocytes/ mL with better quality of the cardiomyocytes exposed to calcium improved was observed empirically (visual comparison of sarcolemmal membranes were straight and bleb-free compared to the higher protease of 5.4 U/mL). Continued reduction of protease from 0.54 U/ mL to 0.06 U/ mL offer did not provide further improvement (decreased to 40 cardiomyocytes/ mL in KB solution; N=2). Next, the length of protease digestion was then reduced over 6 experiments, and it was found that below 20 minutes of protease exposure, no cardiomyocytes could be isolated. We attempted to slightly increase collagenase digestion time to compensate for removal of protease digestion time in 2 experiments, which had negligible effect on the cardiomyocyte isolation.

The resulting enzyme optimization provided a protocol that reliably isolated a mean of 464 cardiomyocytes per mL of KB solution (N=7 rabbits); yet, few

cardiomyocytes were calcium tolerant (mean of 49 cardiomyocytes per mL of NT, N=7 rabbits) or contractile when paced (mean of 4 cardiomyocytes per mL of NT, N=7 rabbits). Poor cardiomyocyte yield was not an adequate for our planned experiments. The few calcium tolerant atrial myocytes that responded to electrical stimulus displayed normal diastolic sarcomere length but poor sarcomere shortening (mean of 1.71 μm and 0.03 μm respectively, n=8 cardiomyocytes). More optimization was required.

2.3.4 Ethylene glycol-bis (β-aminoethyl ether)-N,N,N′,N′-tetraacetic acid

We identified Ethylene glycol-bis (β-aminoethyl ether)-N,N,N′,N′-tetraacetic acid (EGTA) as a target for troubleshooting calcium tolerance and contractile function. While isolated cardiomyocytes have been a powerful model for investigating health and disease, not all methods require contractile myocytes to understand electrophysiological properties, metabolism, or remodelling within the atria. Of note, patch-clamp and voltage/calcium imaging studies aim to specifically avoid contraction, for instance with the use for excitation-contraction uncouplers, such as blebbistatin. EGTA is frequently used at 10 mM concentrations in many cardiomyocyte isolation protocols for its ability to buffer intracellular calcium and as a component in storage/stop solutions to inhibit continued function of digestive enzymes.

EGTA is a poor reagent in isolated cardiomyocyte experiments where contraction is a priority because it decreases the amplitude of calcium transients potentially by blocking L-type calcium channels [94,98]. EGTA can inhibit muscle contraction [99]. In an EGTA-free environment, 30 minutes is insufficient for washout [59]. Therefore, we reduced the largest contributors to EGTA exposure throughout the protocol and adjusted sodium chloride concentrations to maintain isotonicity. As expected, our previous cardiomyocyte isolations displayed variability between experiments and therefore we repeated the same experimental protocol 5 times.

Ultimately, this line of inquiry concluded with our attempts at optimizing our chunk digestion method not resulting in consistent isolation of viable cardiomyocytes. When the experimental protocol was repeated on 5 occasions, only 2 experiments yielded isolated cardiomyocytes in an EGTA-free stop solution. The isolated cardiomyocytes were at a good concentration in stop solution (mean of 553 cardiomyocytes/ mL), but had poor calcium tolerance (mean of 60 cardiomyocytes per mL) and few of these responded to electrical stimulus (mean of 7 cardiomyocytes/ mL), while also displaying shorter than expected diastolic sarcomere length and sarcomere shortening (mean of 1.54 μm and 0.05 μm, respectively, n=4 cardiomyocytes). This removal of EGTA alone did not

improve the health, yield, or calcium tolerance of our isolated cardiomyocytes. Further work is needed to isolate contractile cardiomyocytes by chunk digestion (Table 2).

Table 2: Future optimization for rabbit chunk digestion method

Further optimization	Variable	Potential Benefit	Potential Harm	Reference
1	Temperature	Improves resistance to calcium reintroduction	Alters digestion enzyme activity	100
2	Acidic pH	Decreases contractile ability, energy expenditure and, may act positively on intracellular calcium through Na+/H+ exchanger and NCX	Alters cardiomyocyte and digestive enzyme activity	61,83,100
3	Increase Ca^{2+} concentrations in Digestion solutions towards physiologic levels	Preserves Na+/K+ ATPase activity and minimize calcium reintroduction injury	Prevents the disruption of extracellular junctions and cadherins	52,66,71

2.4 Langendorff perfusion method

After our many attempts at establishing a chunk digestion method failed (7 months of training and 34 experiments and numerous optimizations), we decided to switch to a whole heart digestion method to improve reproducibility and cardiomyocyte viability, as this took precedence. Our lab has extensive experience with Langendorff perfusion, and we have previously shown that Langendorff perfused enzymatic digestion was a reliable way to isolate ventricular myocytes [95].

Hearts were isolated and Langendorff perfused, as described above, using NT bubbled with 100% oxygen. After a rest period of 15 min the perfusate was switched to a wash solution for 10 min, containing (in mM): 117 NaCl, 10 KCl, 1 $MgCl_2$, 10 creatine, 20 taurine, 5 adenosine, 2 L-carnitine, 10 glucose, 10 HEPES, 0.092 EGTA (Sigma-Aldrich), with pH adjusted to 7.40 ± 0.03 with NaOH and an osmolality of 300 ± 5 mOsm/L. The perfusate was then switched to a digestion solution, containing (in mM): 117 NaCl, 10 KCl, 1 $MgCl_2$, 10 creatine, 20 taurine, 5 adenosine, 2 L-carnitine, 10 glucose, 10 HEPES, 0.1 $CaCl_2$ (Sigma- Aldrich), with pH adjusted to 7.40 ± 0.03 with NaOH and an osmolality of 300 ± 5 mOsm/L), to which 200 U/mL Collagenase II (Worthington Biochemical Corporation) and 0.06 mg/mL Protease XIV (from Streptomyces griseus, Sigma Aldrich) was added. After 5 min, the perfusion rate was reduced to 15 mL/min until the atria roughly tripled in size (~15 min). The left and right atria were removed and placed into 25 mL of stop solution, comprised of the digestion solution (without enzymes) and the addition of 0.5 % bovine serum albumin (Sigma Aldrich). The tissue was then cut into 1-3 mm^3 pieces and the solution filtered through a 250 µm nylon mesh. The remaining tissue was returned to 25mL of fresh stop solution, pulled apart with forceps, and the solution was again filtered. The filtered solution was divided into 2 mL Eppendorf tubes and 15 mL Falcon tubes and stored at 4°C.

One mL aliquots of cardiomyocyte containing stop solution were removed from the fridge and the cardiomyocytes left to settle by gravity for 10 minutes. Ten percent of the supernatant was then removed and replaced with NT solution. At subsequent 10-minute intervals, 20%, 50%, and 100% of the supernatant was removed and replaced with NT.

2.5 Patient Inclusion criteria for tissue collection

A non-interventional study application was submitted to the local Research Ethics Board (REB) with collaboration from Dr. John Sapp. Letters of support were submitted

from the requisite departments and division heads. Transportation of Dangerous Goods training was completed by MC in conjunction with a Standard Operating Procedure being submitted to the REB. Dalhousie Legal Services provided a Material Transfer Agreement so tissue samples could arrive to the Sir Charles Tupper Medical Building. Informed consent template was drafted and submitted to the REB.

Patients were identified by the surgery booking office and surgeons were asked if they could be approached by research staff. Research coordinators collected informed consent from interested patients that were undergoing open-heart surgery on a heart lung bypass machine and those patients were considered included in the study.

Subjects (male or female) scheduled to undergo in-patient cardiac surgery at the Halifax Infirmary with the use of a cardiopulmonary bypass system involving peri-operative excision of a piece of right atrial appendage tissue by the cardiac surgeon were considered for inclusion this study. Our exclusion criteria are any previous cardiac surgery or enrolled in another study.

2.6 Patient tissue chunk digestion

Early reported cardiomyocyte isolations from patient tissue were performed by chunk digestion[101]. More recent cardiomyocyte isolations from patient tissues have incorporated a vibratome into a chunk digestion protocol, cannulation of small vessels, or Langendorff perfusion of explanted hearts, in order to improve the number and quality of isolated cardiomyocytes [52,56,59,61]. Isolating atrial myocytes from tissue samples collected during surgery is more difficult than from animal models with only 5-25% of isolated cardiomyocytes having contractile function [84,102]. The total number of viable cardiomyocytes collected would also be expected to be lower than from Langendorff perfused animal models with some groups reporting 19 atrial myocytes isolated per patient sample (n=34) via chunk digestion[103]. While it has been reported that tissue samples weighing between 150 to 600 mg are ideal for atrial myocyte isolations *via* chunk digestion, we collected 210 mg samples on average (N=11)[59,97].

In our study, patients were identified by Nova Scotia Health (NSH) surgery booking for study participation. Included patients had the cannula of the heart-lung bypass machine attached by purse-string-suture, which involves the removal of a piece of atrial appendage.

The following protocol was our final iteration of patient tissue chunk digestions. Atrial samples were immediately placed in ice-cold transport solution, containing (in mM): 142 NaCl, 4.7 KCl, 1 $MgCl_2$, 10 glucose, 10 HEPES, 30 2-3-butadione Monoxime

(BDM), 0.5 $CaCl_2$ (Sigma- Aldrich), with pH adjusted to 7.40 ± 0.03 with NaOH and an osmolality of 330 ± 5 mOsm/L. Transport solutions are frequently modifications of digestion or experimental solutions, and we chose to alter our experimental solution with the cardioplegic capacity arising from sub-physiologic calcium, BDM, and low temperature [52,59,104].

Tissue samples were returned to the lab and rested in ice-cold transport solution for 60 minutes. After the rest period, tissue was transferred to a Sylgard lined dissection dish filled with fresh ice-cold transport solution and pinned across a glass cutting surface with the epicardium side down to minimize stretch of the tissue during the cutting process (Figure 2A). Tissue samples were cut in half with a scalpel with one half being immediately frozen in liquid nitrogen for later western blot analysis. The other half of the atria tissue was cut into 1-3 mm^3 chunks. The chunks of atrial tissue were transferred to a water-jacketed spinner flask (65 RPM) maintained at 37°C filled with calcium free wash solution for 10 minutes, containing (in mM): 102 NaCl, 15 KCl, 1 $MgCl_2$, 10 glucose, 10 HEPES, 10 creatine, 20 taurine, 5 adenosine, 2 L-carnitine, 30 BDM, 0.2% w/v albumin (Sigma- Aldrich), with pH adjusted to 7.40 ± 0.03 with NaOH and an osmolality of 320 ± 5 mOsm/L.

Wash solution was replaced with a calcium containing digestion solution for 30 min, containing (in mM): 102 NaCl, 15 KCl, 1 $MgCl_2$, 10 glucose, 10 HEPES, 10 creatine, 20 taurine, 5 adenosine, 2 L-carnitine, 30 BDM, 0.005 $CaCl_2$, 0.2% w/v albumin (Sigma- Aldrich), with pH adjusted to 7.40 ± 0.03 with NaOH and an osmolality of 320 ± 5 mOsm/L, to which 200 U/mL Collagenase II (Worthington Biochemical Corporation) and 1.4 mg/mL Protease XIV (from Streptomyces griseus, Sigma Aldrich) was added. A custom pipette was used to triturate the tissue chunks in digestion solution for 60 seconds to gently release isolated myocytes. The cardiomyocyte containing digestion solution was filtered through 250 μm nylon mesh to remove the tissue chunks so they could be further digested.

The cardiomyocyte containing digestion solution was gently spun at 100 G for 2 minutes. The supernatant was aspirated and any cardiomyocytes were resuspended in room temperature stop solution, containing (in mM): 102 NaCl, 15 KCl, 1 $MgCl_2$, 10 glucose, 10 HEPES, 10 creatine, 20 taurine, 5 adenosine, 2 L-carnitine, 30 BDM, 0.005 $CaCl_2$, 1% w/v Albumin (Sigma- Aldrich), with pH adjusted to 7.40 ± 0.03 with NaOH and an osmolality of 320 ± 5 mOsm/L. The presence of isolated cardiomyocytes in stop solution was assessed with an inverted brightfield microscope (Olympus, CK2).

The tissue chunks that were filtered and returned to the spinner flask to undergo further enzymatic digestion with only collagenase present. Subsequently, every 15 minutes (at 45, 60, 75 and, 90 minutes of total digestion) the collagenase containing solution was triturated, strained, and exchanged. The subsequent cardiomyocyte containing digestion solutions were spun and resuspended with stop solution, as described above. At the end of 90 minutes of digestion, the remaining tissue chunks were removed with forceps and placed in room temperature stop solution then triturated for 7.5 minutes. Our most successful cardiomyocyte isolation garnered 81 cardiomyocytes in 100 μL of stop solution.

Aliquots at digestion time-points that showed isolated cardiomyocytes under the microscope were selected for calcium reintroduction. Isolated cardiomyocytes were reintroduced to calcium and BDM was washed-out in 10-steps, gradually increasing additions of NT solution. NT was added to the stop solution at 5-minute intervals such that calcium was increased to 0.63%, 1.13%, 2.34%, 4.67%, 9.00%, 14.83% and, 25.89%. At roughly one quarter physiologic calcium it has been reported that isolated cardiomyocytes can be stored for up to two days [52]. We aliquoted isolated cardiomyocytes into 2mL Eppendorf tubes at 25.89% calcium and stored the isolated cardiomyocytes at 4°C. When cardiomyocytes were to be used, they were left on the bench for 10 minutes to reach room temperature and then reintroduced to 45.94%, 57.44%, and 100%calcium at 10-minute intervals. Atrial myocytes isolated in this fashion can be seen in Figure 2B.

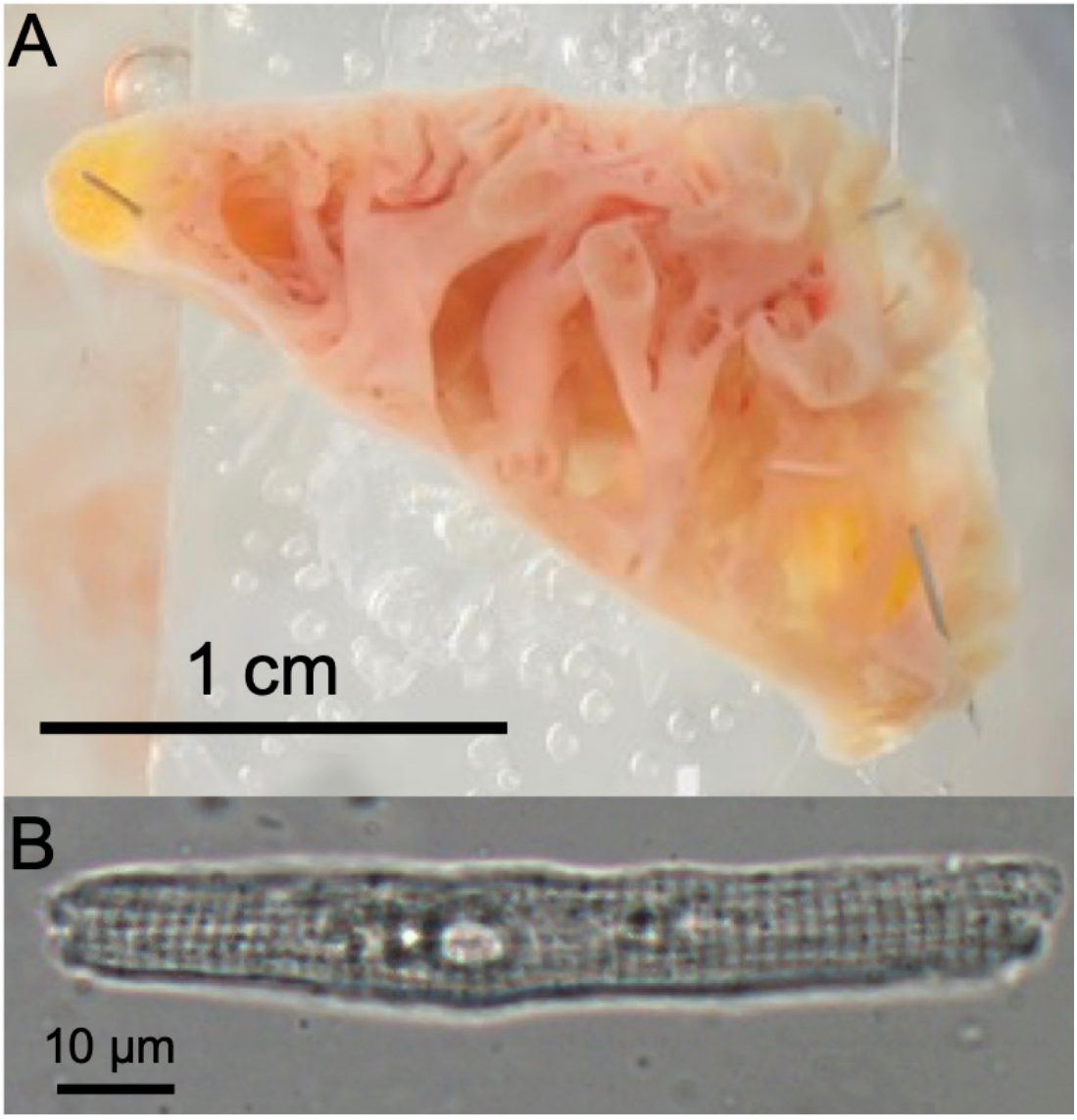

Figure 2: Human cardiac tissue sample and isolated cardiomyocyte A, Image of a right atrial appendage tissue sample weighing 366 mg **B,** Representative isolated human atrial myocyte.

2.7 Patient tissue digestion optimization

While human atrial myocytes have been first isolated over 40 years ago[101], there remains no standardized approach to this method. Patient tissue optimization is inherently more experimentally complex because cardioplegic solutions confer additional variability. Differences in patient pathologies and surgical practices affect cardiomyocyte yield which may require a more conservative approach to cardiomyocyte optimizations [59,61]. Furthermore, the chain of custody of tissue samples is longer in a clinical setting and it can be more difficult to account for temporal effects when comparing between experiments and comparing with the literature.

Table 3 summarises the variables that were considered, the rationale for doing so, how they were manipulated, and the outcome in our attempts to improve our viable cardiomyocyte yield (green = improvement, gray = no change, red = worse).

Table 3: Manipulated variables to optimize patient sample digestion

	Variable	Rationale	Manipulation	Outcome	Reference
1	EGTA Exposure	Calcium buffering with EGTA is protective when isolating myocytes, but impairs calcium transients, contraction, and is difficult to washout	Removal of EGTA from all solutions	Unable to isolate human atrial myocytes	59,93,94
2	Protease Concentration	Disease, age, and species alters time and concentration needed to isolate cardiomyocytes	Increase protease concentration	Isolated cardiomyocytes appear sooner in the digestion	52,59,84,101
3	Digestion chamber	Freeing cardiomyocytes during digestion allows you to check tissue supernatant under the microscope	Digestion in a spinner flask	Provided mechanical disruption during digestion and improved workflow	83
4	BDM Exposure	Chemical phosphatase that inhibits cross-bridge cycling, uncouples excitation, and improves calcium tolerance	Adding BDM to cardioplegic and digestion solutions	Non-contractile calcium tolerant cardiomyocytes	52,97

2.6.1 Cardiac disease and isolation success

Age and disease have been found to affect atrial and ventricular myocyte isolations by requiring more time for tissue digestion [101]. Heart failure decreases the number of isolated cardiomyocytes by up to 40% [61]. Separately, during the collection of patient samples if the atria is clamped during surgery and not purse-string sutured, the number of cardiomyocytes decreases [59].

2.6.2 Enzymes

While we initially anticipated that rabbit chunk isolation would serve as a surrogate for patient tissue isolation, this was not the case. Increasing protease concentration from 0.54 U/ mL back up one order of magnitude to 5.4 U/ mL to that used in the literature yielded more cardiomyocytes by comparision[59,87,97]. While the digestion solution supernatant was initially checked every 15 minutes, starting at 30 minutes of digestion, cardiomyocytes never appeared before 60 minutes of digestion. This was significantly longer than what we would have expected from rabbits. Protocols for atrial appendage chunk digestion can be up to 90 minutes[105].

2.6.3 2-3-Butadione Monoxime

BDM has cardioprotective effects during cardiomyocyte isolations [68]. We observed an improvement in our cardiomyocyte isolation success after logistical issues in the OR resulted in our tissue 'incubating' in BDM containing transport solution for 60 minutes longer than intended. Up to this point we were observing ~2 cardiomyocyte/ 100 µL of digestion solution when the supernatant was assessed. After 60 minutes of BDM incubation, we observed 45 cardiomyocytes / 100 µL (N=2). With an intentional increase in the time of exposure to BDM there was an increase in the yield of striated cardiomyocytes. 10 mM BDM has shown to be protective during cutting of ventricular tissue, but we have yet to try this in the atria[76]. The short transport time from the OR to lab (<15 minutes) may be insufficient for BDM to act upon non-perfused tissue, whereas BDM is effective for others when the transport time from OR to lab is 30-45 minutes [97]. BDM may also be cardioprotective because it is inhibiting NCX through unknown mechanisms[75].

While BDM is extensively used, one group has noted that BDM improves cardiomyocyte viability but may irreversibly inhibit contraction[106]. BDM inhibits L-type calcium currents and if unable to be washed out it continues to inhibit cardiomyocyte contraction[107]. Future optimization in isolating atrial myocytes from patients should include minimization and/or further washout of BDM.

Chapter 3. Experimental methodology

3.1 Carbon fibre method

The mechanical environment of isolated cardiomyocytes can be manipulated[1] using a two Carbon Fibre (CF) method [100]. I used this CF method to apply acute transient axial stretch to atrial myocytes. To mount the CFs, borosilicate glass tubes (5cm long / 1.12 mm inner / 2 mm outer diameter, World Precision Instruments) were pulled into capillaries (PC-1, Narishige) at 68.2°C to ensure the capillary diameter is sized to hold the CF. For the mounted CFs to be aligned near-parallel with the bottom of the cardiomyocyte bath, a 30° bend was placed 1.2 mm from end of the capillary. A CF (12-14 μm in diameter) was then delicately placed in the bent capillary and adhered using cyanoacrylate. A set of CFs were made by trimming the first CF to 1.2 mm and the second CF to 0.6 mm in length from the end of the glass capillary. The longer CF was relatively compliant, used to apply axial stretches, and the shorter CF was relatively stiff, used to hold cardiomyocytes in place.

Determining the stiffness of each CF allowed for the force applied to cardiomyocytes during stretch to be measured. The stiffness of each CF was calculated by pressing a CF against a force transducer (406A, Aurora Scientific) with the output signal recorded by PowerLab (26T, ADI Instruments). The force of the CF against the transducer was averaged over 10 seconds for increasing displacements of the piezo-electric translator (PZT) and, each measurement was performed in triplicate. This data was fit by linear regression to the formula: *stiffness = force / piezo-electric translator displacement*. The force applied during cardiomyocyte stretch was calculated using the recorded CF stiffness and measured piezo-electric translator and CF tip positions (described below), by applying the formula: *force = stiffness * (∆ distance between carbon fibre tips - ∆ distance between piezo-electric translators)*. These formulas were derived from Hooke's Law: $F_s=kx$ [108].

3.1.1 Experimental setup

The CFs contained in capillaries were held in place with a microelectrode holder (MEH820, World Precision Instruments) atop a three-axis water hydraulic micromanipulator (MHW-103, Narishige) for fine-adjustment and myocyte manipulation. This assembly is laterally actuated by a linear piezo-electric translator (P-621.1CD, Physik Instrumente). CF displacement was computer controlled using a piezo amplifier / servo controller (E-665.CR, Physik Instrumente) and driven from a data acquisition (DAQ) device (USB-6361; National Instruments) using custom-routines in LabVIEW

(National Instruments). The PZT sat atop an optical-grade railing system for coarse-adjustment (Figure 3).

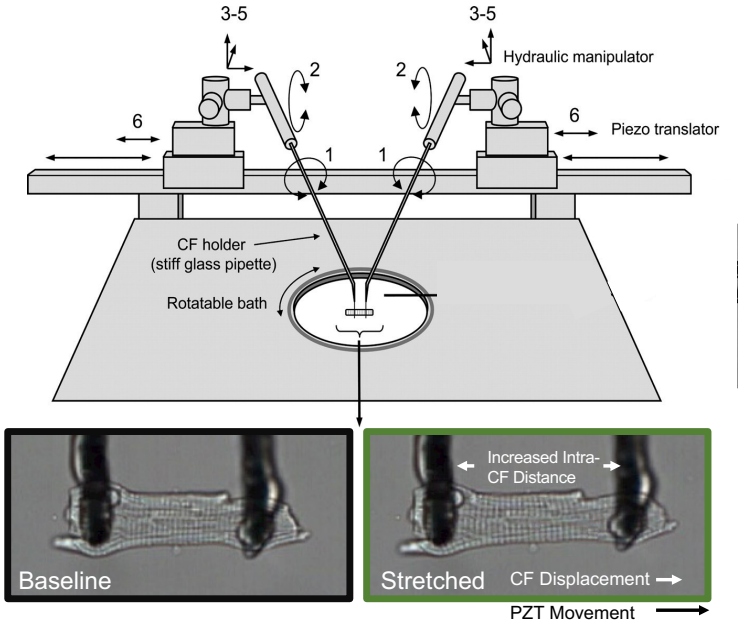

Figure 3. Representation of experimental setup. CFs mounted at the end of glass capillaries are adhered to cardiomyocytes. Capillaries are aligned parallel and held in place with a microelectrode holder atop a hydraulic micromanipulator. These fine-adjustment controls are atop computer controlled PZTs. Optical rails and sledges provide coarse-adjustment. Stretch is applied by lateralling moving the compliant CF *via* displacement of the corresponding PZT. Figure adapted from [109].

Isolated cardiomyocytes resuspended in NT were placed in a 1 mL imaging chamber (RC-27NE2, Warner Instruments) maintained at 35°C by a temperature controller (TC-344C, Warner Instruments). Coverslips in the bottom of the imaging chamber were coated with 30 µL poly-2-hydroxyethyl methacrylate (poly-HEMA; Sigma-Aldrich) to reduce friction between the glass and contracting cells. Cardiomyocytes were visualized with an inverted fluorescence microscope (IX-73, Olympus) with a 40x objective (UPLFLN40X, Olympus).

3.2 Single cardiomyocyte stretch

Atrial myocytes underwent an acute transient stretch protocol that was adapted from previous work [95,109]. After cardiomyocytes in 1.0 mL NT settled to the bottom of the imaging chamber, an electrical pacing stimulus was applied using 1 Hz bipolar electrical field stimulation (100 mA, 2 ms square pulse duration; SIU-102, Warner Instruments). Cardiomyocytes met inclusion criteria if they were rod-shaped with clear striations and well-defined membranes lacked signs of blebbing, and homogeneously contracted when paced. Cardiomyocytes that met inclusion criteria were then randomly selected.

To attach CFs to a cardiomyocyte, the pacing stimulus was paused, and CFs were gently lowered onto either end of the long axis of the cardiomyocyte using hydraulic micromanipulators. CFs adhere to isolated cardiomyocytes through biophysical interactions between the microstructures coating the CF and the sarcolemma [110]. Adhesion between the CFs and cardiomyocytes was confirmed by lifting the adhered cardiomyocyte off the coverslip. Once cardiomyocyte attachment was established, pacing was resumed, and cardiomyocytes were left to contract against the fibres for at least 2 minutes prior to stretching, to improve electrostatic interactions responsible for CF adhesion.

To apply acute transient stretch, the ‘compliant’ CF was moved through lateral translation of PZT by 10 µm of displacement that was applied and removed at a rate of 0.7 µm/ms. A maximum of 3 stretches of 10 µm PZT displacements were applied to cardiomyocyte with stretches spaced apart by 30 second rest intervals (Figure 4A). Stretch was applied during mid-diastole (600 ms delay after an electrical stimulus, Figure 4B). Magnitude of stretch was increased from 10 to 20, 30, and 40 µm PZT displacements and the protocol was repeated. Larger magnitude stretches were excluded due to most cardiomyocytes meeting exclusion prior to, or as a result of, the large stretches (discussed below in limitations section; Figure 12).

The exclusion criteria for cardiomyocytes prior to the application of CF were cardiomyocytes that: spontaneous contracted in the absence of pacing stimulus; that stopped contracting after CF attachment; displayed spontaneous contractions in diastole or, conversely, an absence of contractions in systole during the rest interval between stretches, detached or hypercontracted after any stretch.

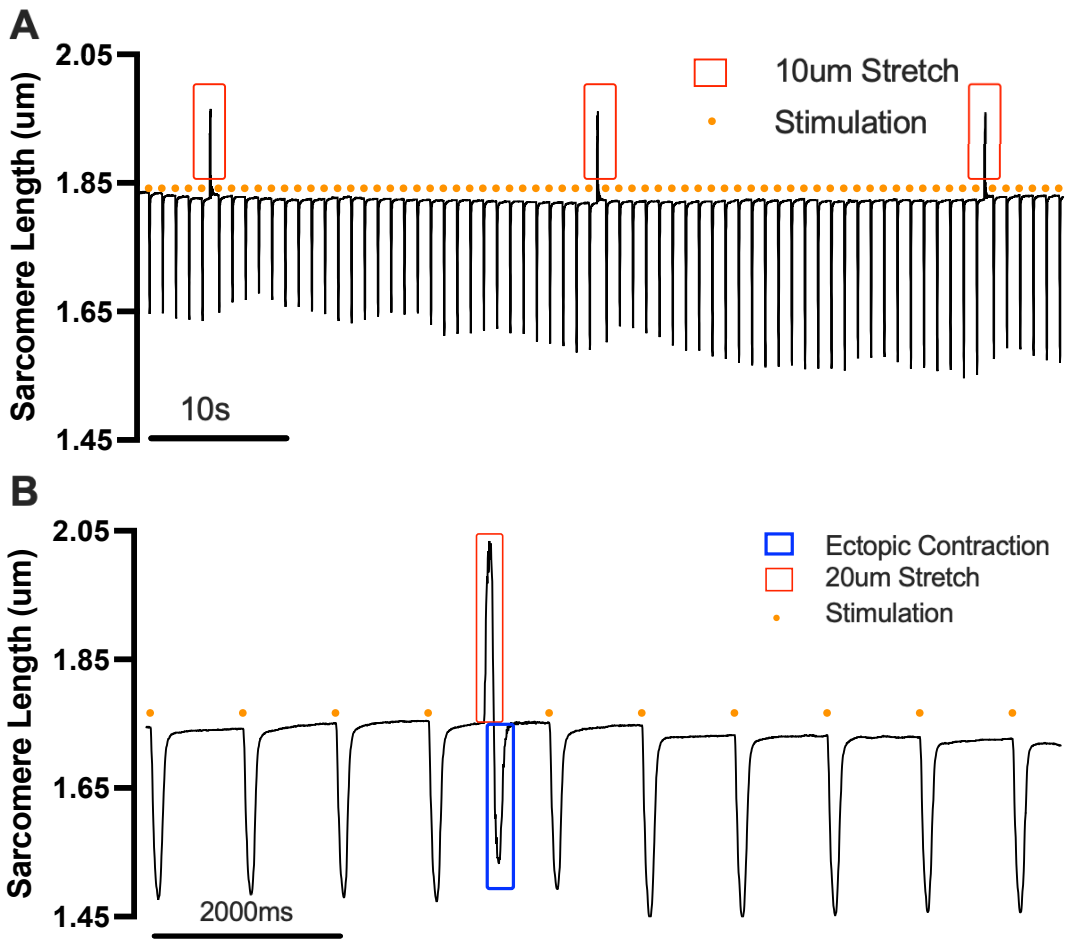

Figure 4. Arrhythmias elicited by rapid, transient stretch of single atrial myocytes. **A,** Sarcomere length tracked over time and is a representation of a stretch protocol, after a cardiomyocyte was paced for at least 2 minutes and then received a 10 μm acute transient stretch. Subsequent stretches were spaced in 30 second intervals. After 3 stretches of 10 μm the magnitude was increased. **B,** Sarcomere length increased during a 20 μm stretch in mid-diastole and a stretch-induced premature contraction occurred.

3.3 Assessment of MA

Sarcomere length, CF, and PZT position was recorded at 250 Hz by video-based monitoring (Myocyte Contractility Recording System, IonOptix) to conduct sarcomere analysis. Sarcomere length was tracked in real time by identifying the high contrast of the sarcomeric z-lines and a Fast Fourier Transform was used to generate a power spectrum indicating the sarcomere length. CF position was monitored by tracking the pronounced contrast between the dark CF and the light background. The IonOptix camera was moderately overexposed to reduce noise levels [110].

Arrhythmic activity was assessed from reviewing sarcomere length measurements, which revealed stretch-induced premature contractions (defined as an unstimulated contraction after stretch) (Figure 4B). The incidence of MA (# stretched induced premature excitations / # stretches) was determined for each pharmacologic intervention.

3.4 Assessment sarcomere dynamics and stretch characteristics

Each cardiomyocyte's contractile dynamics were assessed by measuring the sarcomeric diastolic length, amount of shortening, percentage of shortening and, maximal rate of shortening. Measurements were averaged over 30 paced cycles prior to the first applied stretch in control and pharmacologically treated cardiomyocytes. During the application of stretch, the stretched sarcomere length, percent sarcomere stretch and applied force was measured. Force was then converted to stress by dividing by the unstretched cross-sectional area (CSA), determined by assuming that the cross section is an ellipse with CSA = pi*(width/2)*(thickness/2), with thickness = width/3 [110]. Stretched cardiomyocytes were compared against higher magnitude stretches in control and pharmacologically treated cardiomyocytes.

3.5 Pharmacology

Aliquoted cardiomyocytes in NT received pharmacologic interventions to manipulate factors thought to be important for mechano-arrhythmogenesis based on previous work in the ventricle [95]. Pharmacological agents were dissolved in dimethyl sulfoxide (DMSO) and DMSO was used as a vehicle control (CNTL; 90-minute pre-incubation). In the cardiomyocyte stretch experiments, the order of pharmacologic intervention was block-randomized on the experimental day to mitigate temporal confounding. In cardiomyocyte stretch experiments, once pre-incubations were complete, the solution was replaced with fresh NT and aliquots were only used for cardiomyocyte stretching for 60 minutes.

3.5.1 Paclitaxel

MT were pharmacologically densified and/or detyrosinated in cardiomyocytes with paclitaxel (TAX) (10 μM, 90-minute pre-incubation; Abcam). Other groups have shown that 10 μM TAX (30- minute pre-incubation) increases the amount of MT polymerization in isolated MT [111] and density / detyrosination in ventricular myocytes [16]. In an isolated whole rabbit heart, 5 μM TAX increases the probability of stretch-induced arrhythmias [112].

3.5.2 Parthenolide

MT detyrosination was reduced with parthenolide (PTL) (10 μM, 90-minute pre-incubation; Abcam). Other groups have shown that 10 μM PTL reduces detyrosination and alters mechano-transduction in the rat ventricle[61,113,114].

3.5.3 HC-030031

The small molecule antagonist HC-030031 (HC) was used to block TRPA1 (10 μM, 30-minute pre-incubation; Abcam). Other groups have shown HC to have a 50% inhibitory concentration (IC_{50}) of 6.2 ± 0.2 μM in HEK293 cells [115] and 10 μM HC has been shown to reduces mechanical currents in neuronal cells [32,116].

3.6 Cardiomyocyte immunofluorescence

Immunohistochemistry (IHC) was performed to quantify the density of the MT network in isolated atrial myocytes. Atrial myocytes isolated by the Langendorff perfusion method were reintroduced to calcium through 10%, 20%, 50%, 100% replacements of NT. Due to the large volume and low concentration of the isolated atrial myocytes solution, gravity was insufficient to pellet the cardiomyocytes and replacing the supernatant in these cases decreased cardiomyocyte yield. Therefore, before each calcium reintroduction the cardiomyocytes were centrifuged at 95G for 2 minutes (Sorvall ST 8R, Thermo Scientific) followed by 5-minute wait-period to allow time for pellet formation. This process was repeated for each calcium reintroduction step.

Circular coverslips (22 mm round; VWR) were covered in laminin (100 μg/mL from Engelbreth-Holm-Swarm murine sarcoma basement membrane diluted in PBS, Sigma-Aldrich) and placed in 12-well plates. The coverslips in the wells were covered with 1 mL of isolated cardiomyocytes suspended in NT. Like the stretched cardiomyocytes, the MT were densified/detyrosinated with 10 μM TAX, detyrosinated with 10 μM PTL or, left untreated to incubate and seed for 90 minutes. Experimental conditions were completed in duplicate. The cardiomyocytes were fixed in ice-cold

methanol (stored at -20°C), for 7 minutes at -20°C. Coverslips were rinsed 5 times with phosphate buffered saline (PBS, Sigma-Aldrich) to remove excess methanol.

3.6.1 Antibodies

For staining, coverslips were first blocked in Bovine Serum Albumin (BSA; 5% BSA in PBS, Sigma- Aldrich) at room temperature for 60 minutes. A custom-built humidity chamber was created by stacking 3 Kimwipes soaked in PBS topped with parafilm. Each coverslip was placed onto parafilm cardiomyocyte-side down on 100 µL of primary antibody (1:200, monoclonal rat anti- α-tubulin, MA1-80017, Invitrogen) and stored at 4°C 60 minutes. Coverslips were rinsed 4 times with PBS to remove excess primary antibody. Next, 100 µL of secondary antibody (diluted to 1:500, goat anti-rat IgG, Alexa Fluor 488 conjugate, A-11006, Invitrogen) was added to each coverslip in the chamber for 60 minutes. Coverslips were rinsed 4 times with PBS to remove excess secondary antibody and wrapped in foil to prevent photobleaching. The coverslips were mounted on glass slides using ProLong Glass Antifade Mountant with NucBlue Stain (ThermoFisher). The cardiomyocytes were stored in the 12-well plate at 4°C until imaging.

Imaging of the fixed and stained myocytes was performed on an inverted confocal microscope (TCS SP8, Leica) system with a 40X oil, 1.3 NA objective (HC Plan APOCHROMAT CS2, Leica) and Lightning deconvolution software to obtain high quality images. Samples were illuminated with either 405 nm (for nuclear imaging) or 488 nm (for MT imaging) solid state lasers and visualized with 1.28X zoom and an offset of -0.07. The 405 nm laser used 6.35% intensity and a gain level of 656 with the photomultiplier tube (PMT) detectors set to collect between 410-498 nm. The 488 nm laser used 14% intensity and a gain level of 636 with the PMT detectors were set to collect between 503- 577 nm. A 1.5 µM z-stack of 3 images was obtained. Maximum projections of confocal z-sections were generated using Leica LAS X 3D viewer software.

3.6.2 MT density quantification

Images were then analysed in a blinded fashion using custom software in Fiji (kindly shared by Matthew Caporizzo and Benjamin Prosser, Department of Physiology, University of Pennsylvania Perelman School of Medicine, Philadelphia, USA) to determine MT density, calculated as the fraction of cardiomyocyte area [16]. This software was used to outline the cardiomyocyte and determine a negative background within the cardiomyocyte from regions without immunofluorescence. MT were identified as positive

pixels and MT network was created from the binary image. Poorly identified cardiomyocyte backgrounds would cause apparent degradation of MT in the analysis. MT density was calculated as the MT positive fraction of the total cardiomyocyte area.

3.7 Western blotting

Protein was isolated from right atrial appendages (RAAs) and expression was compared between elevated and normal right ventricular systolic pressure (RVSP) patient populations. The human RAA tissue was ground at cryogenic temperatures in a mortar and pestle. Tissue was homogenized (TissueRuptor II, Qiagen) in fresh NP40-based lysis buffer containing sodium orthovanadate, phosphatase inhibitors (524628, Calbiochem), and protease inhibitors (P8340, Sigma-Aldrich). After homogenization samples were chilled on ice for 30 minutes. Total protein lysate was isolated by 30-minute centrifugation at 1200G (ST8R, Thermo Scientific). Supernatant was collected with a 30-gauge needle to shear DNA. Sample protein concentrations were determined by bicinchoninic acid assay (Pierce BCA protein assay kit, ThermoFisher) and 20 µg of protein per lane was boiled for gel electrophoresis.

Boiled samples were separated (4% stacking gel) and resolved *via* 7.5% sodium dodecyl sulfate-polyacrylamide gel electrophoresis (Mini- PROTEAN SDS-PAGE, BioRad). Samples were loaded alongside a 10 µL protein ladder (Precision Plus Protein Standards Kaleidoscope ladder, BioRad). Self-cast gels (Mini- PROTEAN, BioRad) were run on ice at 90V for 30 minutes and 120V until the dye front migrated to the bottom edge of the gel on ice in Tris/Glycine/SDS electrophoresis buffer (BioRad). Samples were wet-transferred to nitrocellulose (0.2 µm, BioRad) at 100V for 90 minutes while buried in ice. Membranes were briefly rinsed in double-distilled water, and equal protein transfer was confirmed by incubating the membranes in stain (Pierce Reversible Memcode Stain, Thermo Scientific) for 5 min. The stained blot was labeled and imaged (ChemiDoc MP Imaging System, BioRad) before removing the stain (Pierce Stain Eraser, Thermo Scientific). Membranes were then blocked in 5% skim-milk in Tris-Buffered- Saline-Tween 20 (TBS-T, Sigma-Aldrich) for 60 min.

3.5.1 Antibodies

Membranes were incubated at 4°C overnight with α-tubulin (1:1000 monoclonal rat anti- α-tubulin, MA1-80017, Invitrogen) and detyrosinated α-tubulin antibodies (1:1000 mouse anti-detyrosinated α-tubulin, T9154-05H, US Biological Life Science) diluted in 1% skim-milk in TBS-T with sodium azide. Blots were then incubated with secondary antibody (1:3000 horseradish peroxidase HRP- conjugated goat anti-mouse

or goat anti-rat, Jackson Labs) for 120 minutes in 5% skim-milk in TBS-T at room temperature.

3.5.2 Densitometry

Immunoreactivity was then measured (Clarity Western Enhanced Chemiluminescence Substrate, with a ChemiDoc MP Imaging System, BioRad). Membranes were stripped by incubation in 25 mL of 0.5 M Tris-HCl/SDS buffer supplemented with 125 µL 2-mercaptoethanol (Sigma-Aldrich) for 1 hour and re-probed. Densitometric quantification was done using Image Lab (6.0.1, Bio-Rad). Values were obtained by measuring the target band relative to the total protein of reference one lane from a patient sample that was conserved between gels.

3.6 Statistics

All statistics and graphing were performed in Prism 9.0 with a significance of $p<0.05$. The categorical variable of MA incidence was assessed with a two-sided Fischer's Exact test. The continuous variables related to sarcomere dynamics, applied stretch, MT density, and protein expression had differences between group means assessed. In all cases, a normality test was applied and subsequently, two-way ANOVA with Tukey *post hoc* tests (for normally distributed data) or Kruskal-Wallis tests with Dunn's multiple comparisons test (for data that was not normally distributed) were used. For paired data, a mixed effect analysis with Tukey's *post hoc* test was used to account for missing data due to cardiomyocytes meeting exclusion criteria. The relevant test and number of replicates is indicated in each figure caption. N = rabbits, n = cells, m = stretches.

3.7 Human and animal ethics statement

Rabbit experiments were conducted in accordance with the ethical guidelines of the Canadian Council on Animal Care, with protocols approved by the Dalhousie University Committee for Laboratory Animals.

The NSH research ethics board approved this research (REB # 1026599), and informed consent was obtained for all participating patients. All personal identifiers were stripped prior to data analysis to ensure patient anonymity and confidentiality.

Chapter 4. Results

4.1 MT density/detyrosination alters atrial MA in a TRPA1-dependent manner

To determine the MA of atrial myocytes, we applied acute transient stretch to cardiomyocytes isolated from rabbit hearts and determined the incidence of stretch-induced ectopy. The incidence of stretch-induced arrhythmias was altered by exposures to MT densification agents, MT detyrosination inhibitors, or TRPA1 blockers. For cardiomyocytes in CNTL conditions, an increase in the amount of PZT displacement (10 *vs* 20 μm) did not alter the incidence of MA (3% vs 0%; $p>0.999$; Figure 5). Contrarily, in cardiomyocytes treated with MT densification agent TAX, there was an increase in MA incidence at the larger PZT displacement (1% *vs* 9%; $p=0.0183$), indicating a potential change in the MA threshold that was not reached in CNTL cardiomyocytes. Coincubation of TAX with MT detyrosination inhibitor PTL prevented the increase in MA incidence with increased PZT displacement that occurred with TAX alone (0% *vs* 4%; $p=0.283$). Similarly, coincubation of TAX with TRPA1 blocker HC also prevented the increase in the incidence of MA (1% *vs* 4%; $p=0.564$). Together this data suggests a stretch magnitude threshold for MA exists, which is reduced by TAX, but mitigated by PTL or HC.

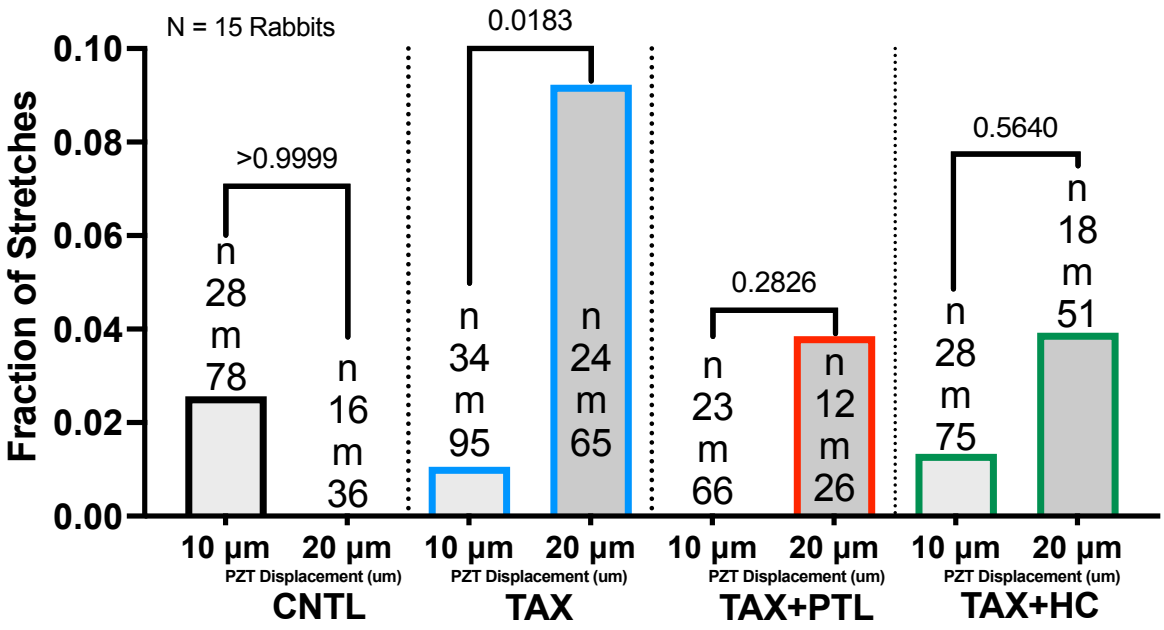

Figure 5: Effect of microtubule manipulation and HC-030031 (TRPA1 blocker) on mechano-arrhythmogenic threshold (MA). Incidence of MA (# stretched induced premature excitations / # stretches) with acute transient stretch at increasing amount of piezoelectric displacement in rabbit isolated atrial myocytes in control (CNTL; black), exposed to paclitaxel alone (TAX, 10 µM for 90 min; blue), or in combination with parthenolide (PTL, 10 µM for 90 min; red) or the TRPA1 blocker HC-030031(HC, 10 µM for 30 min; green). Differences were assessed using chi-square contingency tables and Fisher's exact test within a treatment condition, exact *p*-values shown. N = rabbits, n = cells, m = stretches.

4.2 Acute stretch characteristics during pharmacological manipulations

As the magnitude of stretch appears to be important for MA incidence with TAX, with the effect altered by our pharmacological manipulations, we wanted to determine if the mechanical characteristics of stretch experienced by the atrial myocytes changed with the degree of PZT displacement, and if our interventions altered that relationship. Applied stress, maximal stretched sarcomere length, and percentage change in sarcomere length during stretch all increased with an increase in PZT translation for all treatment conditions. Applied stress with 10 and 20 μm PZT displacement increased in CNTL from 4.24±0.29 to 7.44±0.70 mN/mm^2 (p<0.001), in TAX from 4.97±0.30 to 8.66±0.65 mN/mm^2 (p<0.001), in TAX+PTL from 3.48±0.22 to 7.83±0.91 mN/mm^2 (p<0.001), and in TAX+HC from 4.04±0.40 to 8.11±0.81 mN/mm^2 (p<0.001; Figure 6A). Maximal stretched sarcomere length increased in CNTL from 1.82±0.01 to 1.90±0.03 μm (p=0.009), in TAX from 1.84±0.01 to 1.92±0.02 μm (p<0.001), in TAX+PTL from 1.74±0.02 μm to 1.80±0.02 μm (p=0.03), and in TAX+HC from 1.81±0.02 to 1.90±0.03 μm (p=0.005; Figure 6B). Percentage change in sarcomere length increased in CNTL from 5.4±1.1 to 9.1±1.4% (p=0.008), in TAX from 5.8±0.5 to 11.0±0.9% (p<0.001), in TAX+PTL from 6.0±0.8 to 12.9±1.6% (p<0.001), and in TAX+HC from 5.2±0.5 to 10.0±1.4% (p=0.001; Figure 6C). This shows that the characteristic of the stretch experienced by the cardiomyocyte scales with PZT displacement.

To determine if stretch characteristics are altered by our pharmacological interventions, we compared values between treatment conditions. For 20 μm PZT displacement, no differences in applied stress were found (Figure 6A). Interestingly, the detyrosination inhibitor PTL decreased the maximal stretched sarcomere length compared to TAX (Figure 6B; p=0.012), however when normalized against resting diastolic sarcomere length, there were no differences in percentage sarcomere stretch between the conditions (Figure 6C) , reflecting a shorter diastolic sarcomere length with TX+PTL (see below for a consideration of the effects of the pharmacological agents on mechanical function). For 10 μm PZT displacement, TAX+PTL similarly decreased maximal stretched sarcomere length compared to TAX, but in that case also compared to CNTL (Figure 6B; p=0.0032 and p<0.0001, respectively). Taken together, this indicates that PTL may mitigate the increase in MA during acute stretch with TAX, presumably by altering the cytoskeletal network.

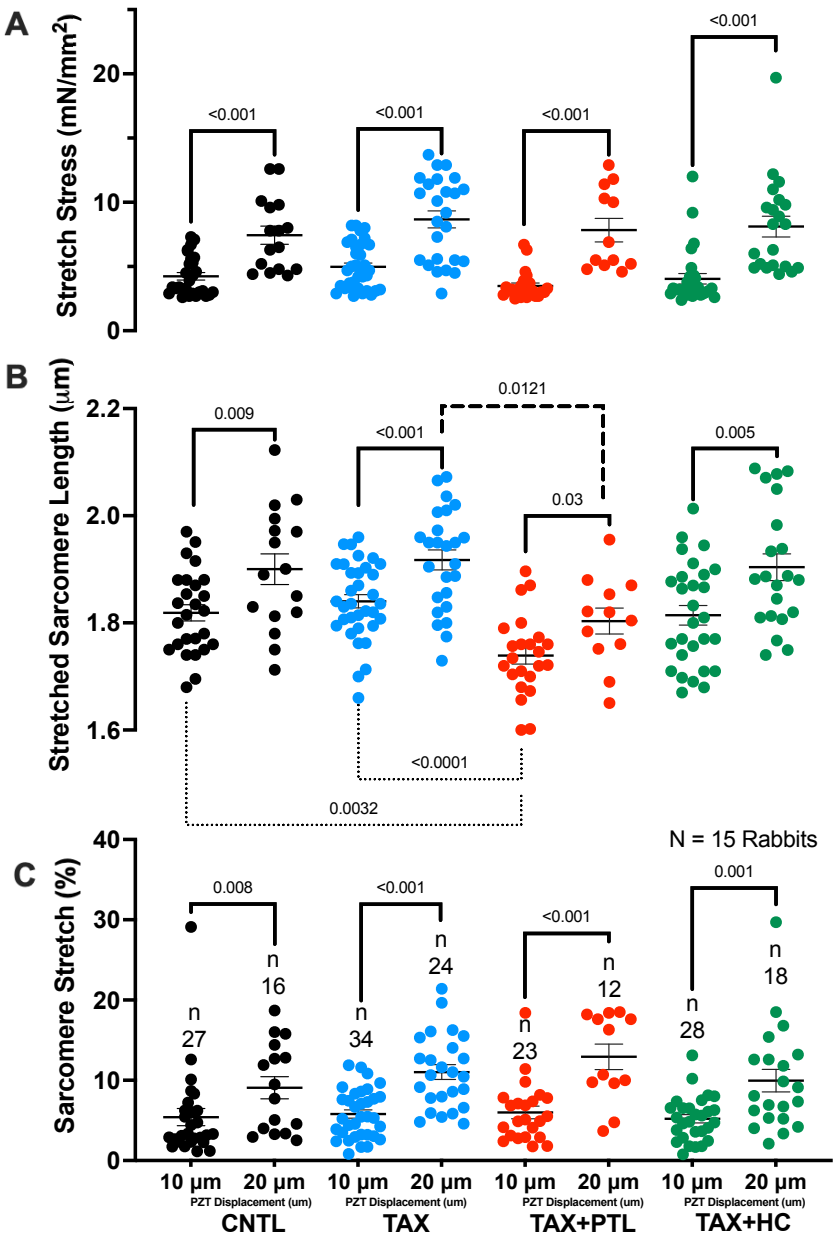

Figure 6: Mechanical characteristics of acute cardiomyocyte stretch in response to pharmacological manipulations. A, Applied stress; **B,** maximal stretched sarcomere length; and **C,** percentage change in sarcomere length during the application of acute transient stretch in isolated rabbit atrial myocytes with an increased degree of PZT displacement in control cardiomyocytes (CNTL; black) and cardiomyocytes exposed to paclitaxel (TAX, 10 μM for 90 min; blue), TAX +parthenolide (PTL, 10 μM for 90 min; red), or TAX +HC-030031 (HC, 10 μM for 30 min; green). Differences within treatment conditions assessed with unpaired t-tests or Mann-Whitney tests (solid bars). Normality testing was performed and subsequently dictated the type of test applied. Differences between treatment conditions for 10 μm (dotted bars) and 20 μm (dashed bars) PZT displacements were assessed by one-way ANOVA with Tukey's *post hoc* comparisons and Kruskal-Wallis with Dunn's *post hoc* comparison. Error bars represent standard error of the mean. N = rabbits, n = cells.

We were also interested in comparing stretch characteristics between atrial and ventricular myocytes (using data for rabbit ventricular myocytes obtained in a previous study by Dr. Breanne Cameron). Data for stretch of atrial myocytes in CNTL (with 10 and 20 μm PZT displacement) are plotted alongside the lowest magnitudes of stretches applied to ventricular myocytes (20 and 30 μm PZT displacement). At 20 μm PZT displacement, atrial myocytes were subjected to a higher level of cardiomyocyte stress than ventricular myocytes (Figure 7A; 7.34±0.67 *vs* 3.63±0.11 mN/mm^2; $p<0.001$), even though ventricular myocytes experienced a greater degree of maximal stretched sarcomere length (Figure 7B; 1.89±0.13 *vs* 1.97±0.09 μm; $p=0.03$). When normalised, however, there is no difference in percentage change of sarcomere length during stretch (Figure 7C; 8.8±1.3 *vs* 8.3±0.7%; $p=0.82$). Thus, greater stress may contribute to a greater MA incidence with smaller PZT displacements in atrial myocytes compared to ventricular myocytes.

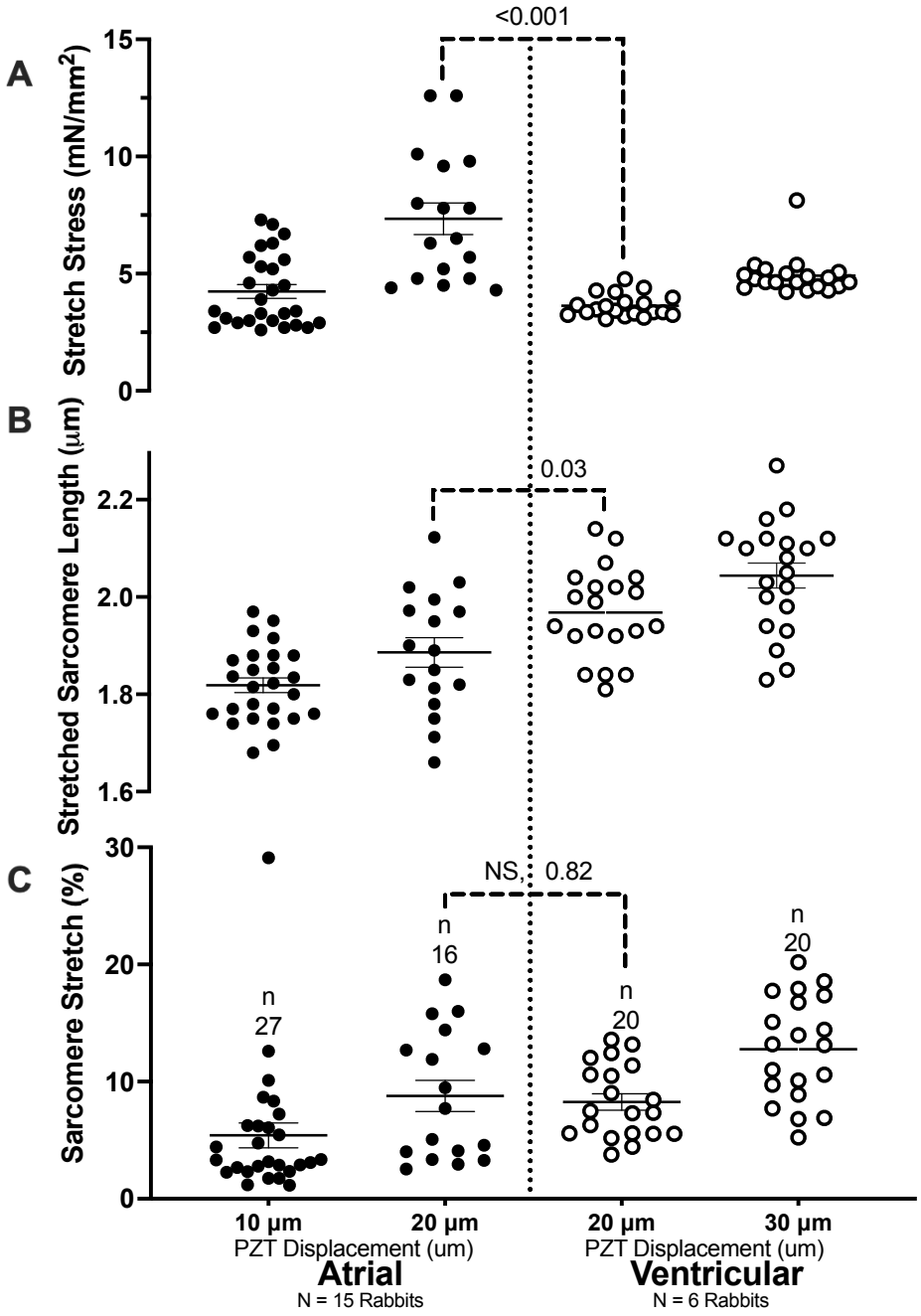

Figure 7: Mechanical characteristics of acute stretch in atrial and ventricular myocytes. A, Applied stress; **B,** maximal stretched sarcomere length; **C,** percentage change in sarcomere length during the application of acute transient stretch in rabbit isolated atrial (black) and ventricular (white) myocytes with an increasing amount of PZT displacement in control conditions. Normality testing was performed and subsequently dictated the type of test applied. Differences assessed between cardiomyocyte types at equivalent 20 μm PZT displacements using Mann-Whitney or unpaired t-test. Error bars represent standard error of the mean. N = 15 rabbits, n = cells.

4.3 MT detyrosination alters cardiomyocyte contractile dynamics

We were also interested in determining if our pharmacological interventions affected characteristics of cellular mechanical function. The coincubation of TAX with the detyrosination inhibitor PTL decreased the average diastolic sarcomere length (1.68±0.014 μm) compared to CNTL (1.75±0.009 μm; p=0.002), TAX (1.75±0.008 μm; p=0.0002), and TAX+HC (1.74±0.015 μm; p=0.005; Figure 8A). There was no difference in absolute sarcomere shortening during contraction between the treatment conditions (CNTL = 0.12±0.008 μm, TAX = 0.15±0.010 μm, TAX+PTL = 0.18±0.019 μm, and TAX+HC = 0.14±0.011 μm; Figure 8B), but percentage shortening was greater for TAX+PTL (10.9±1.1%) compared to CNTL (7.0±0.5%; p=0.005) and TAX+HC (8.0±0.6%; p=0.046; Figure 8C). There was no difference between TAX+PTL and TAX (8.5±0.6%; p=0.475). It was also found that the maximal rate of sarcomere shortening is greater in the TAX+PTL treatment (-4.4±0.5 μm/s) compared to CNTL (-2.5±0.2 μm/s; p=0.004; Figure 8D), while there was no difference with TAX (-3.2±0.2 μm/s; p= 0.6627) or TAX+HC (-3.0±0.2 μm/s; p= 0.203). Regarding the maximal rate at which the sarcomeres lengthen during relaxation, there were no differences between the treatment conditions. Overall, altered contractile dynamics occur with application of PTL, perhaps due to reduced cytoskeletal attachments to the sarcomere caused by inhibition of MT detyrosination leading to decreased resistance during contraction.

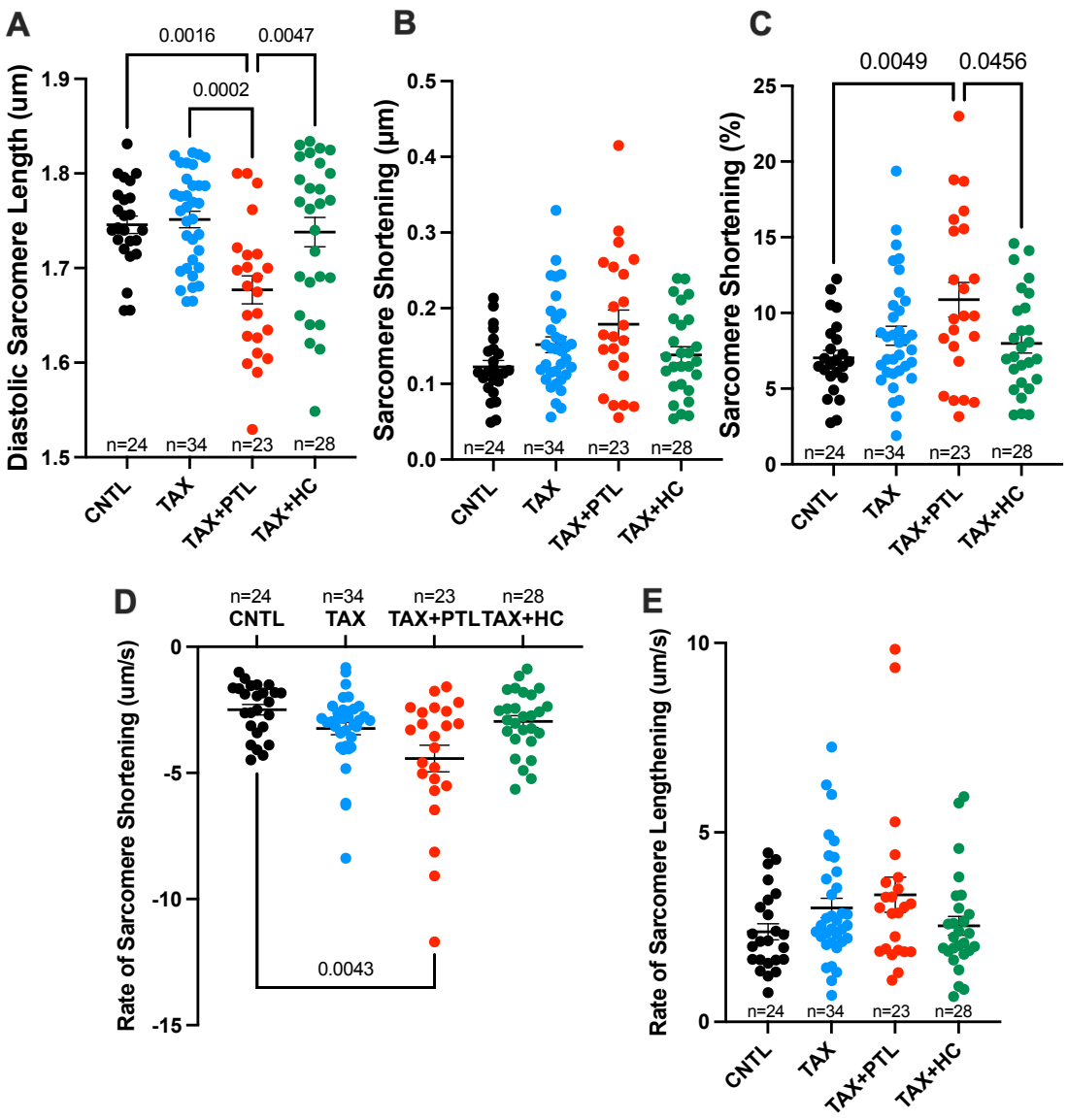

Figure 8: Effects of pharmacological interventions on contractile function. A, Diastolic sarcomere length; **B,** absolute sarcomere shortening; **C,** percentage sarcomere shortening; **D,** maximal rate of sarcomere shortening and **E,** lengthening at the end of 2 minutes of paced contractions (1 Hz) in rabbit isolated atrial myocytes in control (CNTL; black) and with paclitaxel (TAX, 10 µM for 90 min; blue), TAX+parthenolide (PTL, 10 µM for 90 min; red)or TAX+HC-030031 (HC, 10 µM for 30 min; green). Values were averaged over 30 cycles. Normality testing was performed and subsequently dictated the type of test applied. Differences were assessed between treatment conditions by Kruskal-Wallis with Dunn's post hoc comparison and one-way ANOVA with Tukey's post hoc comparison. Error bars represent standard error of the mean. N = 15 rabbits, n = cells.

Similarly, we were also interested in whether the application of repeated acute stretches had an effect on the contractile function of the atrial myocytes. To investigate this, we compared measures of contractile function (diastolic sarcomere length, absolute and percentage sarcomere shortening, maximal rate of sarcomere shortening and lengthening) in the same CNTL cardiomyocytes at sequential intervals: pre-stretch, after the first stretch with 10 μm PZT displacement, and after the third stretch (Figure 9). There was no apparent change in any contractile parameters from pre-stretch values after one stretch. Three stretches, however, may have some effect. While not significantly different, a reduction in diastolic sarcomere length after three stretches (1.73±0.012 μm) compared to pre-stretch (1.74±0.009 μm) and post-one stretch (1.75±0.009 μm) could be appreciated (Figure 9A; p=0.055 and 0.054, respectively). The same was observed for an increase in absolute and percentage sarcomere shortening after three stretches (0.147±0.014 μm and 8.5±0.8%) compared to pre-stretch (0.122±0.009 μm and 7.0±0.5%; Figure 9B & 9C; p=0.065 and p=0.059). The maximal rate of sarcomere shortening was significantly increased when comparing three stretches (-3.4±0.4 μm/s) to one stretch (-2.8±0.3 μm/s; Figure 9D; p=0.027) and the maximal rate of sarcomere lengthening after three stretches (3.1±0.4 μm/s) was increased compared to pre-stretch (2.4±0.2 μm/s; Figure 9E; p=0.014). The close to significant change in diastolic sarcomere length may indicate that with repeated stretches there was CF slippage or cardiomyocyte buckling. The gain of function in sarcomere shortening and lengthening after repeated stretch could indicate altered ion handling through an unknown mechano-sensitive mechanism.

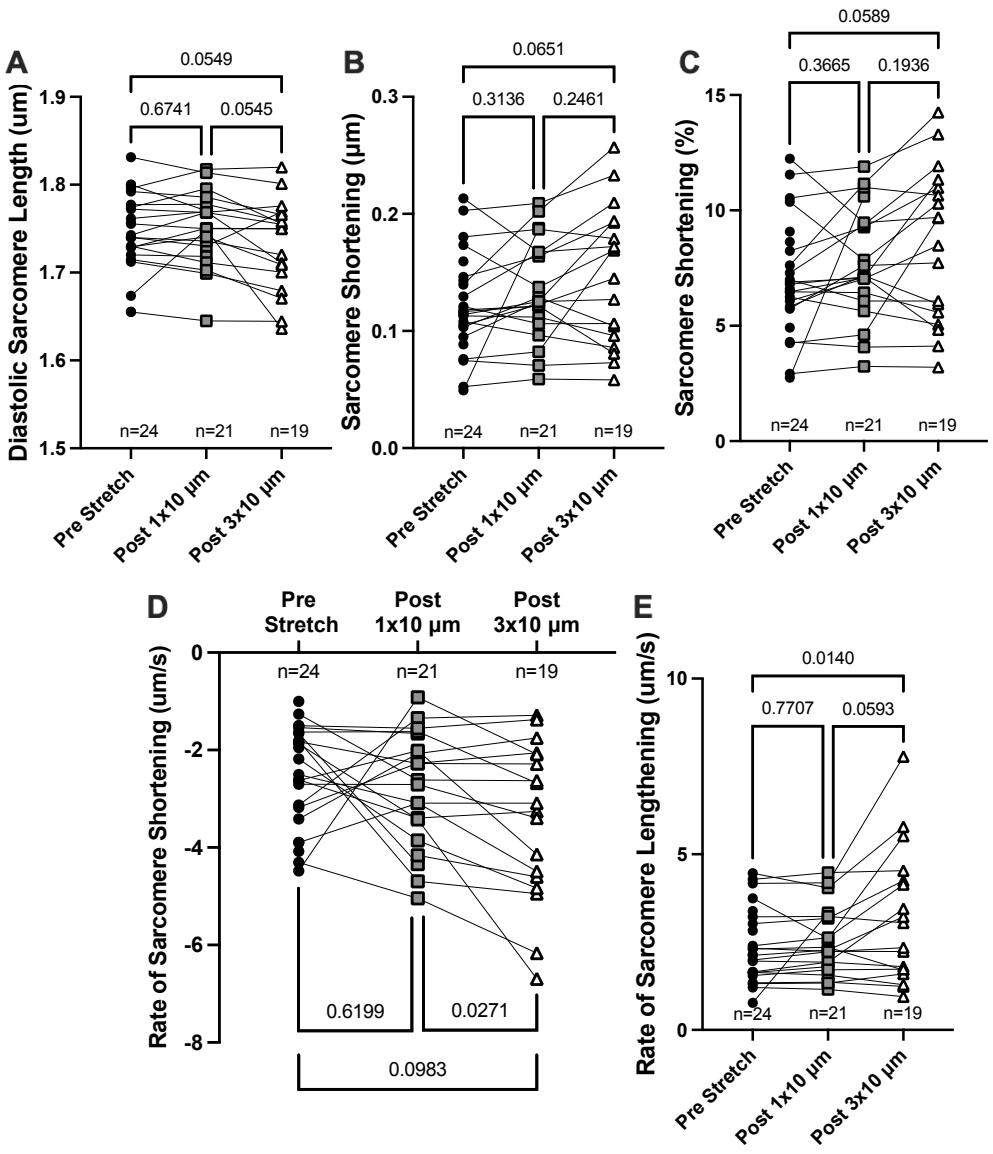

Figure 9: Effects of repeated acute stretch on contractile function. A, Diastolic sarcomere length; **B,** absolute sarcomere shortening; **C,** percentage sarcomere shortening; **D,** maximal rate of sarcomere shortening; and E**,** maximal rate of sarcomere lengthening in rabbit isolated atrial myocytes exposed to control conditions. Sarcomeres were assessed pre-stretch at the end of 2 minutes of paced contractions (1 Hz) averaged over 30 cycles, after the first stretch with 10 µm PZT displacement averaged from cycle 10 to cycle 20 post stretch, and after three stretches averaged from cycle 10 to cycle 20 post stretch in the same cardiomyocyte and compared by mixed effect analysis with Tukey's *post hoc* tests to account for missing data due to cardiomyocytes meeting exclusion criteria. N = 15 rabbits, n = cells.

4.4 MT density is altered by TAX

To assess whether alterations in the MT network are driving the increase in MA incidence with TAX, we used immunofluorescence to measure MT density in CNTL, TAX, and TAX+PTL treated cardiomyocytes. Representative images of myocytes with stained α-tubulin are seen in Figure 10A, which were analyzed to determine the MT positive fraction of total cardiomyocyte area to quantify MT density. TAX increased MT density compared to CNTL (Figure 10B; 67.0±1.3% *vs* 55.9±2.2%; p=0.002). Coincubation of TAX with detyrosination inhibitor PTL, which promotes the degradation of MT, decreased MT density compared to TAX (Figure 10B; 57.7±2.9% *vs* 67.0±1.3%; p=0.012). Thus, MT density may play a key role in increasing MA incidence, with detyrosination being an important mitigator of MT density and MA incidence.

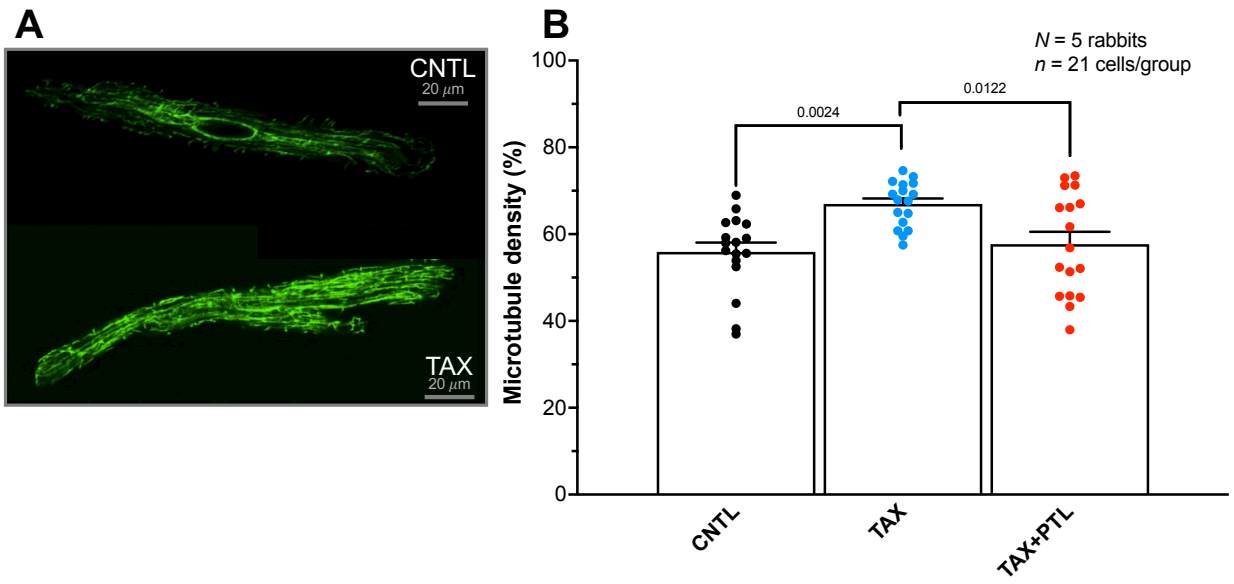

Figure 10: Effect of pharmacological interventions on microtubule density A, Representative confocal immunofluorescence images of microtubules in control (CNTL) and paclitaxel-treated (TAX) atrial myocytes. **B** Microtubule density assessed as the microtubule positive fraction of the total cardiomyocyte area in control (CNTL; black) and after exposure to paclitaxel (TAX, 10 μM for 90 min; blue) or TAX+parthenolide (PTL, 10 μM for 90 min; red). Error bars represent standard error of the mean. Differences were assessed by one-way ANOVA with Tukey's *post hoc* tests. N = rabbits, n = cells.

4.5 Patient characteristics

Aim 2 was focused on translating our approach into human atrial myocytes isolated from tissue samples collected from cardiac surgery patients to determine if patients with right-sided pressure overload (right ventricular systolic pressure, RVSP, >35mmHg) had altered MA due to changes in MT. While we were ultimately unable to isolate contractile atrial myocytes, we did still assess patient characteristics, echocardiographic parameters, and MT protein expression. Of the twelve patients that met inclusion criteria, 9 patients had normal RVSP ($\leq$35mmHg) and 3 had right-sided pressure overload (classified as pulmonary hypertension). The demographic characteristics are shown in Table 4.

Table 4 Patient demographics. Values displayed as counts and percentages, unless indicated as mean and standard deviation (SD). Chi-square and Fisher's exact test comparisons were performed for frequency distributions. Mann-Whitney tests were used for comparison of continuous variables. AVR, aortic valve replacement; CABG, coronary artery bypass graft; MVR, mitral valve replacement.

Right Ventricular Systolic Pressure							
	Normal (< or =35mmHg) N=9		**Elevated (> or =35mmHg)** N=3			**All** N=12	
	n	%	n	%	**p**	n	%
Mean Age (SD)	*59.44*	*(14.41)*	*63.33*	*(23.03)*	*0.73*	*60.42*	*(15.83)*
Male Sex	5	(56)	2	(66)	>0.99	7	(58)
Mean Resting Heart Rate (SD)	*70.34*	*(13.94)*	*73*	*(11.53)*	*0.77*	*71*	*(12.92)*
Hypertension	5	(56)	1	(33)	>0.99	6	(50)
Atrial arrhythmia	0	(0)	*1*	(33)	0.25	*1*	(8)
Ventricular arrhythmia	1	(11)	0	(0)	>0.99	1	(8)
Antihypertensives	8	(89)	2	(66)	0.45	10	(83)
Antiarrhythmics	1	(11)	0	(0)	>0.99	1	(8)
Indication for Surgery:							
CABG	8	(89)	1	(33)	0.1006	9	(75)
AVR	1	(11)	1	(33)		2	(17)
MVR	0	(0)	1	(33)		1	(8)

4.5.1 Echocardiographic data

To assess whether elevated RVSP patients had undergone cardiac remodelling we compared echocardiographic parameters between patient groups. Elevated RVSP patients had increased left atrial volumes (LAV, indexed to body size) compared to normal pressure patients (Table 5; 50.6 mL/m^2 *vs* 25.2 mL/m^2; p=0.01) and increased left ventricular end systolic diameter (LVESD) (Table 5; 5.50 cm *vs* 3.29 cm; p=0.05). There may also be a relationship between elevated RVSP and left ventricular (LV) posterior wall thickening (normal = 0.96 cm *vs* elevated = 1.10 cm), as the comparison almost reached significance (p=0.09). Overall, this data shows that cardiac remodelling has occurred in elevated pressure patients on the left side of the heart, which may thus also be occurring on the right side of the heart including changes in MT density and detyrosination.

Table 5 Echocardiographic parameters of normal and elevated right ventricular pressure patients. Values displayed as counts and percentages, unless indicated as mean and standard deviation (SD). Fisher's exact test comparisons were performed for frequency distributions. Mann-Whitney tests were used for comparison of continuous variables. LV, left ventricle; LVEF, LV ejection fraction; LA, left atria; LAV, LA volume; LVESD, LV end systolic diameter (LVESD); LVEDD, LV end diastolic diameter. Not a Number (NaN) shown for missing values.

Right Ventricular Systolic Pressure							
	Normal (< or =35mmHg) N=9		**Elevated (> or =35mmHg)** N=3			**All** N=12	
	mean	SD	mean	SD	**p**	mean	SD
LV Posterior Wall (cm)	0.96	0.11	1.10	0.10	0.09	1.00	0.12
LV Septum (cm)	1.04	0.30	1.13	0.06	0.63	1.07	0.26
LVEF (%)	36.45	11.36	38.67	19.76	0.77	37.40	14.00
LAV indexed (mL/m^2)	25.18	9.03	50.63	9.95	**0.01**	34.73	15.76
LA Diameter (cm)	3.88	0.92	NaN	NaN	NaN	3.88	0.92
LVESD (cm)	3.29	1.01	4.70	0.40	**0.05**	3.71	1.09
LVEDD (cm)	4.81	1.05	5.50	0.20	0.30	5.00	0.94
Estimated RV systolic pressure (mmHg)	28.23	3.81	52.35	1.34	0.01	37.88	13.50

4.6 MT and detyrosinated MT expression in elevated and normal pressure patients

As MT density and/or detyrosination status appear to be important for MA incidence in rabbit isolated atrial myocytes, we wanted to assess if patients with elevated RVSP show evidence of MT changes. Protein analysis was performed to determine if there was a difference in expression of MT and detyrosinated MT with RVSP status (Figure 11). The expression of detyrosinated α-tubulin, α-tubulin, and the ratio of detyrosinated / α-tubulin was not different between normal and elevated RVSP patients ($p=0.21$, $p=0.61$, and $p=0.48$ respectively), but we are currently underpowered for these comparisons.

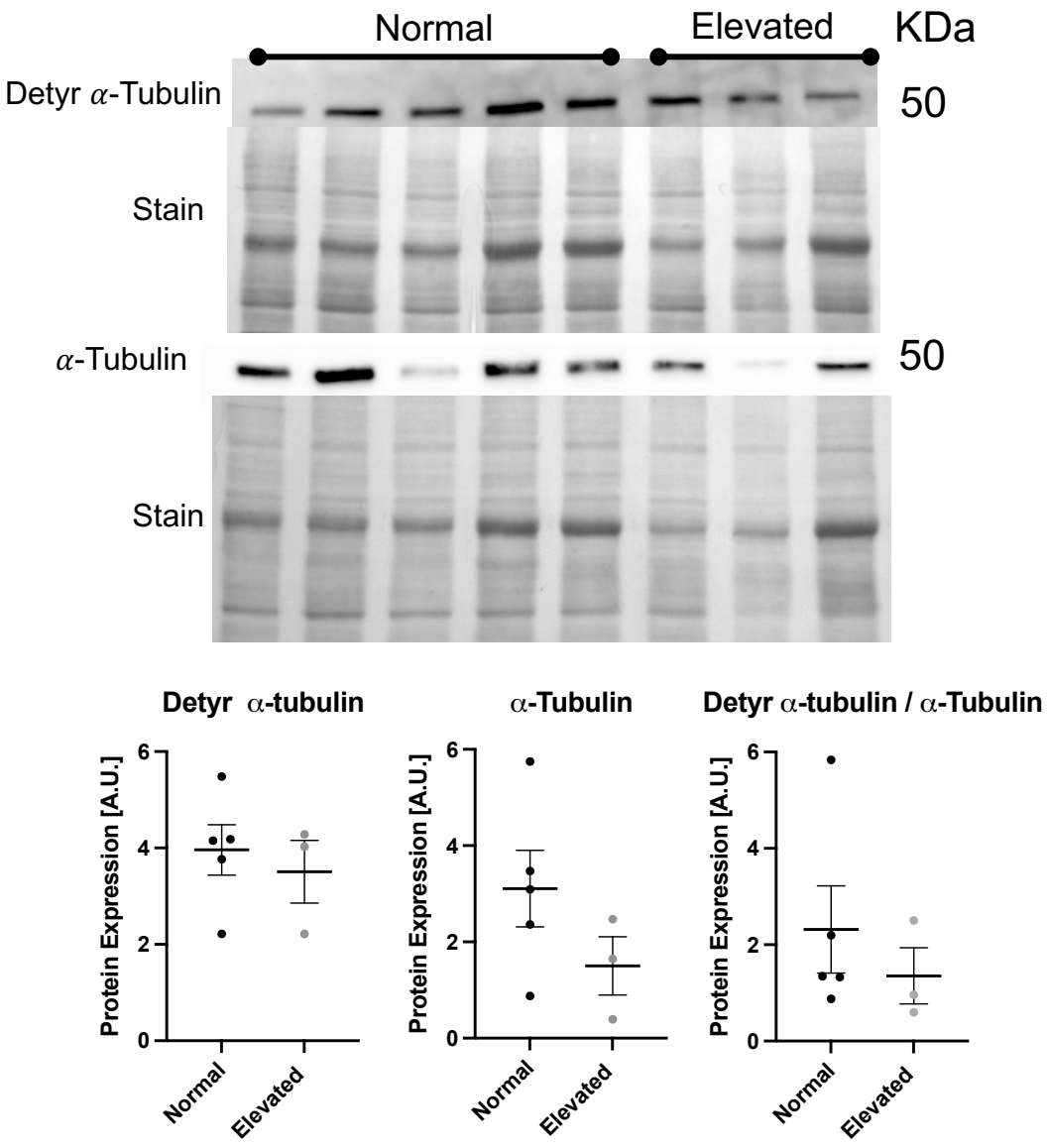

Figure 11: Effect of elevated right heart pressure on microtubule expression and detyrosination status Western blot analysis of detyrosinated ∝-tubulin and ∝-tubulin with Memcode whole protein stains. Normal pressure patients have RVSP ≤35mmg and elevated pressure patients an RVSP ≥35mmHg. Error bars represent standard error of the mean.

Chapter 5. Discussion

In my thesis, I sought to determine the contribution of MT and TRPA1 to MA in the atria by subjecting isolated atrial myocytes to controlled acute transient stretch. I showed that MT density and detyrosination status affect MA in a TRPA1-dependant manner. Specifically, I showed that increased MT density by exposure to TAX leads to an increased incidence of MA as the magnitude of stretch is increased. Inhibiting detyrosination with PTL mitigated this increase, potentially by decreasing MT density and/or their direct linkages to sarcomeres. Blocking TRPA1 channels with HC-030031 also mitigated the TAX-induced increase in MA, suggesting that stretch-induced excitation involves TRPA1 (Figure 5).

5.1 MT density and detyrosination determine MA threshold in atrial myocytes

It has been shown previously that there is an increase in the incidence of MA with an increase in the magnitude of acute transient stretch in rabbit isolated ventricular myocytes. This relationship, however, appears to have a minimum stretch threshold, as in control conditions it was not until stretch magnitude went above a certain value (associated with a PZT displacement of 40 μm in those experiments) that an increase was seen. 8% from vs 0% at 30 μm)[117]. When ventricular myocytes were exposed to TAX, this threshold appeared to shift downward, as an increase in MA incidence occurred instead with a PZT displacement of 30 μm (9% *vs* 1% at 20 μm). From the present study, it appears that an MA threshold is also present in isolated atrial myocytes, which is similarly lowered by TAX. While in control conditions there was no increase in MA with 10 or 20 μm PZT displacements, after the addition of TAX an increase was seen (from 1% to 8%; Figure 5). Importantly, while here we have shown that similar to ventricular MT densification—where with TAX increases MA incidence—the increase in MA occurred at lower magnitudes of stretch in the atria (20 μm) than in the ventricle (30 μm). This suggests that a different MA threshold is present in atrial compared to ventricular myocytes. More work is needed to determine if a MA threshold can be observed at large PZT displacements in atrial myocytes under control conditions.

The post-translational detyrosination of tubulin promotes linkages between MT and the sarcomeres *via* desmin[12,21]. In both previous studies in ventricular isolated myocytes and the present study in atrial myocytes, coincubation of TAX with PTL, which reduces detyrosination, mitigates the increase in MA incidence associated with TAX. There was no change in MA incidence with increased PZT displacement in the atria (Figure 5) or the ventricle[11] when detyrosination was inhibited. This decrease in MA with

the inhibition of detyrosination further supports the role of MT as mechano-electric transducers that contribute to MA.

In the previous ventricular work, in some cases stretch resulted in complex self-sustained arrythmias that lasted for multiple seconds before spontaneously resolving; this did not occur with stretch of atrial myocytes, in which only ectopic contractions were observed (Figure 4B). The mechanisms of the sustained arrhythmic activity in ventricular myocytes remain unclear [117], but the difference between ventricular and atrial myocytes may be explained by a lower capacitance or sodium / calcium currents in atrial myocytes, which has been shown to exist in cardiomyocytes isolated from mouse [118]. Furthermore, sodium currents inactivate faster and at more negative membrane voltages in rabbit isolated atrial myocytes compared to ventricular myocytes, which may additionally contribute to the absence of complex arrhythmias in response to stretch [119]. Alternatively, it is possible that stretching atrial myocytes at larger magnitudes may result in complex sustained arrhythmias.

5.2 TRPA1 is a mechano-electric effector of atrial MA

We believe the mechano-sensitive TRPA1 channels are mechano-electric effectors in the heart that can drive atrial MA *via* a depolarizing calcium influx. In previous studies using ventricular myocytes [117], and with atrial myocytes in the present study, coincubation of TAX with HC mitigated the increase in MA incidence associated with TAX, as there was no change in MA incidence with increased PZT displacement in either atrial (Figure 5) or ventricle myocytes [117]. In fact, experimental and clinical evidence exists for a contribution of TRPA1 to atrial fibrillation, as TRPA1 KO mice have decreased arrhythmia incidence with pulmonary irritant exposure[120] and there is an increase in TRPA1 (although measured in leukocytes) in non-valvular atrial fibrillation patients[51]. The contribution of TRPA1 to MA, however, may depend on engagement of MT. It has been observed that there is no increase in TRPA1 current with stretch of the sarcolemmal membrane by negative pressure during patch clamping [121,122], suggesting that MA may be driven by an interaction between MT and TRPA1 during acute stretch.

5.3 MT density and detyrosination alter viscoelastic properties of atrial myocytes

Analysis was performed to assess how the characteristics of stretch differs at different stretch magnitudes and if this effect is modulated by our pharmacologic interventions. Increased PZT displacement increased stretch stress, stretched sarcomere length, and percent sarcomere stretch for all experimental groups. Stretch characteristics were similar across the groups after the pharmacological interventions,

except for stretched sarcomere length, which was lower in the TAX+PTL group, due to a decreased diastolic sarcomere length (described below; Figure 6). Importantly, this shows that there are no differences in acute stretch characteristics between the pharmacologic interventions in atrial myocytes that could account for the differences in MA.

In our acute transient stretch model, the same rate of stretch was used for atrial and ventricular myocyte stretch. For the same magnitude of PZT displacement in the two cardiomyocyte-types, there was a greater stress in the atrial myocytes (7.34 *vs* 3.63 mN/mm^2), while the percentage stretched sarcomere length was similar (8.8% *vs* 8.3%; Figure 6). Thus, the stress associated with acute stretch in atrial myocytes is greater than in ventricular myocytes, which may indicate differences in their MT network.

In ventricular myocytes there is a difference in the effect of TAX on stretch characteristics compared to atrial myocytes. TAX exposed ventricular myocytes displayed a decrease in percent sarcomere stretch compared to control (12 *vs* 16% and 16 *vs* 22% for 30 and 40 μm PZT displacement, respectively)[117], while there was no difference for atrial myocytes (Figure 6). This difference between atrial and ventricular myocytes remained consistent with the coincubation of TAX with PTL. There was no difference in percent sarcomere stretch between TAX+PTL and control conditions in atria myocytes (Figure 6), but TAX+PTL exposed ventricular myocytes displayed a decrease in percent sarcomere stretch compared to control (13 *vs* 16% and 17 *vs* 22% for 30 and 40 μm PZT displacement, respectively)[117]. Taken together, our results show that with similar stretch, there is greater stress in atrial *vs* ventricular myocytes, and that there is greater percent sarcomere lengthening after TAX exposure in atrial myocytes, suggesting that atrial myocytes may have different mechanical properties that contribute to observed differences in MA between the two cardiomyocyte-types. This difference could relate to differences in the organization of the MT network between atrial and ventricular myocytes, as it has been shown that MT alignment confers stiffness in cardiomyocytes[12]. More work is needed, however, to determine the elastic properties and Young's Modulus of atrial and ventricular myocytes during acute stretch.

5.4 MT density and detyrosination alter mechanical function of atrial myocytes

Our atrial myocytes isolated using a Langendorff perfusion technique had similar contractile properties to atrial myocytes isolated using a newer, vibratome based technique. In control conditions, the two methods produced atrial myocytes with a comparable diastolic sarcomere length (1.75 μm *vs* 1.71 μm), sarcomere shortening (7%

vs 8%), maximal rate of sarcomere contraction (-2.50 µm/s *vs* -1.95 µm/s), and lengthening (2.38 µm/s *vs* 1.75 µm/s) [52]. Thus, we believe our isolated atrial myocytes are healthy and representative of normal isolated atrial cardiomyocyte contractile dynamics.

In the present study, reducing MT detyrosination with PTL was shown to mitigate the TAX-induced increase in MA and affect atrial myocyte contractile dynamics. Previous work in our lab found no changes in contractile function of ventricular myocytes with application of PTL alone[117], while in rat isolated ventricular myocytes treated with PTL, there was an increased rate of sarcomere shortening and lengthening (and a decrease in sarcomere shortening and lengthening with TAX) [17,25]. While I did not test the effect of PTL alone in atrial myocytes, in our rabbit isolated atrial myocytes, TAX alone had no effect on contractile dynamics and there was an increase in the rate of sarcomere shortening with TAX+PTL (Figure 8D), again suggesting differences exist between atrial and ventricular myocytes.

PTL alone has been shown to cause no change in diastolic sarcomere length in rat ventricular myocytes [17,47]. A decrease in linkages between the cytoskeleton and sarcomeres, in combination with TAX-induced alterations of viscoelastic properties, may explain why diastolic sarcomere length was decreased in atrial myocytes exposed to TAX+PTL in our experiments (Figure 8A). Decreased resistance due to limited sarcomere cytoskeleton interactions seen with TAX+PTL in atria myocytes resulted in increased percentage sarcomere shortening (Figure 8C), and TTL overexpression (to increase reattachment of tyrosine residues to detyrosinated tubulin) in rat isolated ventricular myocytes resulted in increased absolute sarcomere shortening [21,23]. Taken together, decrease linkages between the sarcomeres and the cytoskeleton with PTL appear to decrease resistance to contraction.

We also sought to assess whether effects of acute stretch on contractile function was causing cell damage. Single stretches did not alter contractile function, however there was a surprising improvement in function (rather than a decrease, as would be expected from cell damage) with repeated stretches. The rate of sarcomere shortening was increased after repeated stretches compared to single stretches (-3.4±0.4 µm/s *vs* -2.8 µm/s; Figure 9D), as was the rate of lengthening (3.1 µm/s *vs* 2.4 µm/s; Figure 9E). In contrast, single and repeated stretches had no effect on contractile function in ventricular myocytes [117]. Cyclic stretch applied with a different rate than acute transient stretch causes stretch-induced alterations trans-sarcolemmal ion handling and

concentrations as well as viscoelastic stiffness [1]. The effect of repeated acute transient stretch in atrial myocytes observed here may driven by the same mechanisms of cyclic stretch.

5.5 Effects of pharmacological interventions on MT density

To assess the effects of TAX and PTL on the MT network in atrial myocytes, MT density analysis was performed. MT density was increased with TAX exposure compared to control (66% *vs* 55%; Figure 5), which was like that seen previously in the ventricle (66% *vs* 59%) [117]. Whilst in rat isolated ventricular myocytes there was no significant effect of TAX on MT density [17]. In the present study, co-incubation of rabbit atrial myocytes with TAX and PTL prevented the increase in MT density, as seen previously in ventricular myocytes. Unfortunately, we were unable to co-stain detyrosinated MT to assess changes during TAX and TAX+PTL exposure due to the unavailability of appropriate secondary antibodies. In previous studies using rat isolated ventricular myocytes, it was found that TAX increased the fraction of detyrosinated MT, which was decreased by either PTL or TTL overexpression [17,21].

The differences in effects on MT between TAX+PTL and PTL alone could be due to tyrosinated MTs being more dynamic, less stable, and being degraded in the presence of PTL [22]. Analysis of MT organisation could be used to better understand differences in how changes in MT alter non-linear viscosity in atrial and ventricular myocytes and its possible role in MA.

5.6 Patient echocardiography and MT protein expression may indicate remodelling in patients with elevated RVSP

Unfortunately, we were unable to isolate contractile atrial myocytes from open-heart surgery patients but using frozen tissue samples we were able to assess protein expression. Increased MT density is associated with an in increase in α-tubulin protein expression[17]. We sought to differentiate the expression of α-tubulin and detyrosinated α-tubulin between patients with normal and elevated RVSP. The increases in left atrial volume and LVESD in our limited patient population may indicate that cardiac remodelling has occurred in the left side of the heart in elevated RVSP patients. Pressure overload has been shown previously to increase left and right atrial volume [123,124]. However, the estimated RVSP in our limited elevated RVSP cohort (52±1 mmHg) is much lower than that reported previously by others (82±20 mmHg[124] and 81±23 mmHg[125]). The relatively low RVSP pressure within our elevated pressure cohort may

mitigate the differences we saw in protein expression between normal and elevated RVSP patients.

If atrial structural remodelling has occurred in response to pressure overload, then we might expect to observe differences in MT expression [126]. We did not observe differences in α-tubulin or detyrosinated α-tubulin between the two groups, but our limited patient numbers meant we lacked statistical power for these comparisons. Western blots of ventricular tissue from normal and heart failure patients in previous studies have shown that α-tubulin is increased in hypertrophic cardiomyopathy, dilated cardiomyopathy, and ischemic cardiomyopathy, indicating a potential role of α-tubulin remodelling [16]. More work is needed to determine how pressure overload affects MT in the atria and if this may contribute to MA incidence as seen in our rabbit model.

5.7 Limitations

5.7.1 Mechano-electric mediators

The contribution of mechano-electric mediators to atrial MA was not investigated in this body of work. Future work could benefit from understanding the changes to mechano-electric mediators and MA in response to atrial pathophysiology.

5.7.2 Hierarchical statistical modelling

Common practice in isolated cardiomyocyte studies is to assume that each cardiomyocyte is an independent data point, irrespective of the animal it came from [84]. While common practice, each isolated cardiomyocyte may in fact not be independent, as experimental variability may result in differences between cardiomyocyte isolations that make cardiomyocytes from each not fully independent, leading to artificially low p-values and inaccurate conclusions (false positives or type 1 errors) [127,128]. A more conservative approach to address dependency between myocytes for each cardiomyocyte isolation is to average results from cardiomyocytes for each. Averaging cardiomyocytes from each isolation, however, goes against convention, reduces statistical power, visual richness of the data, and increases the number of animals and experiments required. Alternatively, hierarchical statistical modelling can be used to reduce type 1 errors by calculating the amount of clustering of cardiomyocytes from one animal and artificially altering the SEM. An SEM from a hierarchical test would fall between a test where all *cardiomyocytes* were treated as independent and a test where all *animals* were treated as independent. Highly clustered data from cardiomyocytes, due to variability in cardiomyocyte isolation, would have an SEM trending towards values similar to independent animals. Statistics

packages are becoming standardized and open-sourced in R to better reflect intra-animal comparisons [129,130]

5.7.2 Carbon fibre slippage

A limitation of our CF-based stretch system is that cardiomyocytes begin to detach as PZT displacement is increased to larger levels. Moreover, in our experience, it is more difficult to apply acute stretch to atrial myocytes compared to ventricular myocytes, in which higher magnitudes of stretch can be attained before detachment. With atrial myocytes, cardiomyocytes were generally successfully stretched with below 30 μm PZT displacement, at which point stretch success began to drop (Figure 12A). The difficulty in stretching cardiomyocytes at large displacements was the rationale to exclude these incomplete datasets. To determine if the ability to successfully apply a protocol of three stretches in one cardiomyocyte, the number of stretches delivered (m) was normalized to the number of cardiomyocytes stretched (n). It was more difficult to repeatedly stretch cardiomyocytes at larger magnitudes, as with repeated stretches cardiomyocytes became detached from the CFs (Figure 12B).

A more complex CF-based system using four CFs, with one above and below the cardiomyocyte at each end could be used to apply larger PZT displacements without detachment from the cardiomyocyte. In previous studies, 16% greater sarcomere stretch was applied to mouse isolated ventricular myocytes using a four compared to two CF-based system [131].

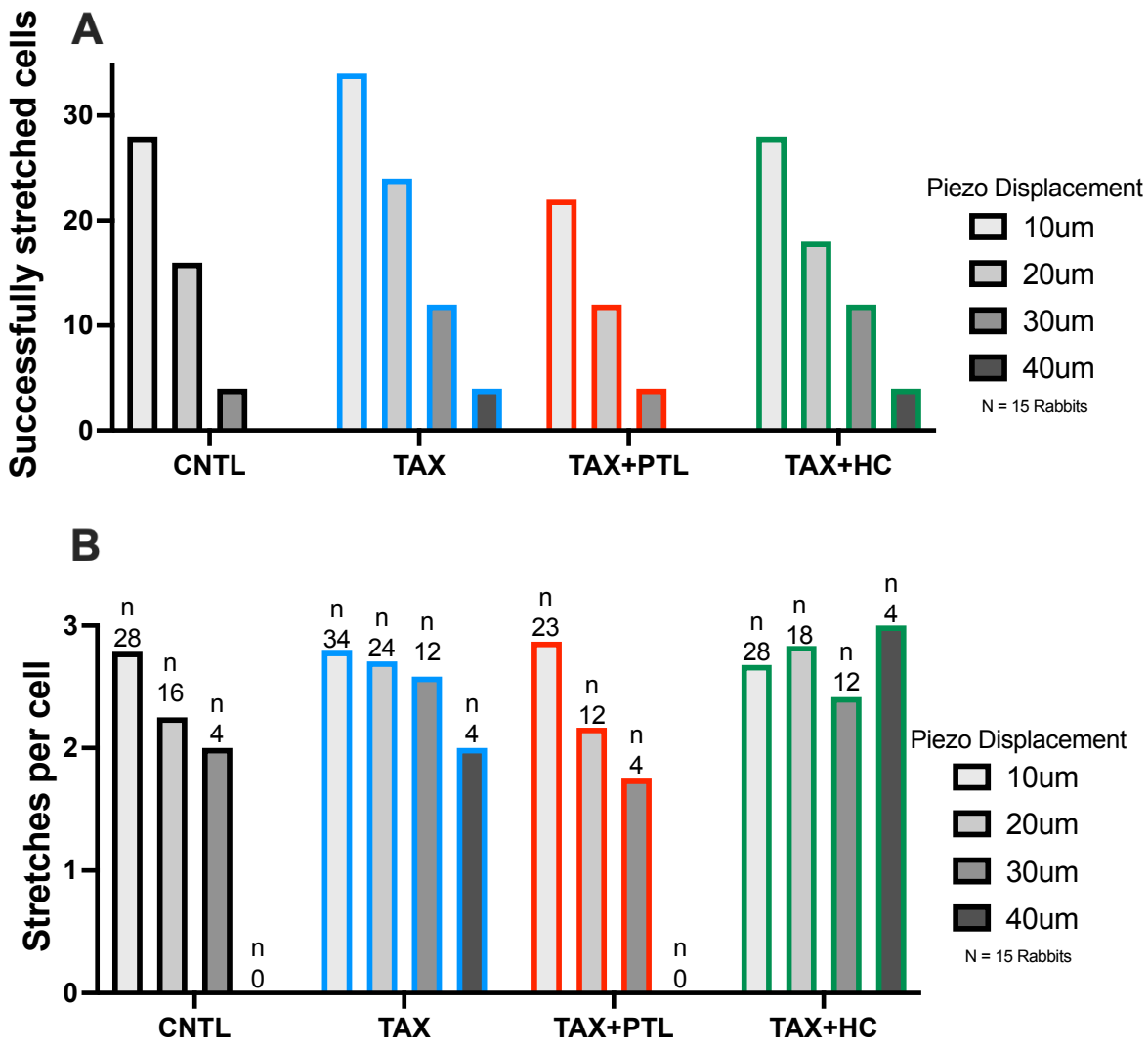

Figure 12: Effect of increasing piezo displacement on successful cardiomyocyte stretches A, Successfully stretched cardiomyocytes **B,** Successful stretches per cardiomyocyte for all attempted PZT displacements and between treatment conditions. Successful stretches per cardiomyocyte = total number of stretches / total number of cardiomyocytes.

5.7.3 Sequential stretch order

During the stretch protocol, stretch was applied at increasing magnitudes of PZT displacement (10, 20, 30, then 40 μm), rather than in a randomised order. This method was applied because of the decreased likelihood of successfully stretching cardiomyocytes at 30 and 40 μm. The sequential stretch order may contribute to confounding temporal effects of repeated stretch, such as effects on contractile function (Figure 9). More work is needed to determine if the observed changes in function are solely driven by repeated stretch or if time between stretches plays a role.

5.7.4 Antibodies

Use of a detyrosinated tubulin antibody would have allowed for direct measurement of the density of detyrosinated MT. Unfortunately, previously published work in rats and human made use of rabbit polyclonal anti-detyrosinated tubulin antibodies, which are unsuited for use in rabbits [16,17]. Measuring detyrosinated MT and the ratio of detyrosinated/total MT density could have allowed us to determine combinatorial effect of TAX+PTL on MT degradation and MT density.

We also aspired to directly measure changes in TRPA1 expression between patients and determine subcellular localization in rabbits. There are no validated TRPA1 antibodies for use in rabbits, and only limited mouse monoclinal anti-TRPA1 antibodies [132]. Results of our monoclonal mouse anti-TRPA1 clone 6G8 immunohistochemistry analysis resulted in staining that appears more similar to non-specific background staining than successfully stained plasma membrane channels [133]. The manufacturer references a publication using a rabbit polyclonal anti-TRPA1 antibody in western blotting to support the efficacy of their mouse monoclonal anti-TRPA1 6G8 [134], however the monoclonal mouse anti-TRPA1 6G8 clone (WH0008989M3; Sigma-Aldrich) did not work in our hands in western blotting, even after extensive optimization.

5.7.5 Patient inclusion

While patient recruitment was severely impacted by the COVID-19 pandemic, we were still able to recruit some patients at the Halifax Infirmary (internal communication)[135], though patient recruitment was limited to the available in-patient surgery population. Thus, the included patients may not be representative of the greater population of pressure overload patients. Furthermore, our limited patient group appears to not be representative of cardiac surgery patients as a whole, as our population was younger and had a higher proportion of female patients than that expected from the literature [136,137].

Also, the size of our atrial samples was on the lower end of that recommended for cardiomyocyte isolation, and of the collected tissue approximately half was reserved for protein analysis. Thus, future work may benefit from larger tissue samples if available.

5.8 Future directions

More work is needed to further investigate the interaction between MT, MA threshold, and TRPA1 in the atria using a four CF-based stretching apparatus. Replicating this work in a chronic pressure overload rabbit model could be foundational for isolated human cardiomyocyte experiments from pressure overload patients. The role of chronic pressure overload on remodelling of MT density, MT post-translational modifications, and TRPA1 expression could further elucidate their contribution to MA in cardiac disease. Chronic remodelling may reflect differences in MT density and detyrosination seen with TAX and PTL. A potential relationship between chronic remodelling and MA is promising, as PTL has been shown to decrease stiffness and improved contractile function in ventricular myocytes from heart failure patient [16].

Identification of TRPA1 and detyrosinated α-tubulin antibodies suitable for IHC staining could allow for co-localization of these proteins to further determine their interactions. Additionally, the causative relationship between TRPA1 and MA could be further investigated in both rabbit isolated atrial and ventricular isolated myocytes by developing a nanoparticle encapsulated siRNA TRPA1 knockdown to potentially mitigate MA [138].

5.8.1 MA assessment in patient cardiomyocytes and pharmacological interventions

If left atrial appendectomies become the standard of care, then more tissue mass may be available to digest via the chunk method in the future and more cells could be isolated. If tissue samples remain the same size, then maintaining patient tissue in more physiologically similar solutions, removing BDM, and using temperature as the only cardioprotective agent could result in contractile myocardial preparations. It has been shown that removing digestive enzymes and preparing 3-6 mm atrial myocardial muscle bundles in cold modified KH solution maintains contractile tissues from atrial appendages [139]. A similar method could be adapted to deliver acute stretch using a linear servomotor and then MA incidence could be assessed. A reliable MA model in patient tissue would increase sample sizes so a univariate logistic regression model can be generated to account for differences in patient history. Further potential benefits of a

successful atrial myocardial muscle bundle preparation would be potential experimental parity with a rabbit model and a reduction in research animal usage.

Future clinical significance of this work could include risk stratification for episodes of atrial fibrillation in the setting of elevated cardiac filling pressures (*e.g.*, hypertension, heart failure, valvular heart disease). Determining drivers of MA may reveal novel targets for future anti-arrhythmic therapies that have improved side effect profiles by acting on mechano-electric transducers or effectors, like MT or TRPA1.

Chapter 6. Conclusion

Here we have shown that MT density and detyrosination both play a critical role in atrial MA, through a TRPA1-dependent mechanism. Different viscoelastic properties of atrial and ventricular myocytes may contribute to altered MA thresholds. Sarcomere-cytoskeletal linkages affect myocyte contractile function and non-linear viscoelasticity. MT are important mechano-electric transducers that may play a role in cardiac remodelling and atrial arrhythmia. Future work should determine the overall contribution of MA to atrial arrhythmias to decrease the burden of atrial fibrillation.

References

1. Alexander Quinn T, Kohl P. Cardiac mechano-electric coupling: Acute effects of mechanical stimulation on heart rate and rhythm. *Physiological Reviews* [Internet]. 2021 [cited 2022 Apr 13];101:37–92. Available from: https://journals.physiology.org/doi/full/10.1152/physrev.00036.2019
2. Bers DM. Cardiac excitation–contraction coupling. *Nature 2002 415:6868* [Internet]. 2002 [cited 2022 May 2];415:198–205. Available from: https://www.nature.com/articles/415198a
3. Eisner DA, Caldwell JL, Kistamás K, Trafford AW. Calcium and Excitation-Contraction Coupling in the Heart. *Circulation Research* [Internet]. 2017 [cited 2022 Jun 26];121:181. Available from: /pmc/articles/PMC5497788/
4. Quinn TA, Kohl P, Ravens U. Cardiac mechano-electric coupling research: Fifty years of progress and scientific innovation. Progress in Biophysics and Molecular Biology. 2014;115:71–75.
5. Ravens U. Mechano-electric feedback and arrhythmias. *Progress in Biophysics and Molecular Biology*. 2003;82:255–266.
6. Taggart P, Sutton PMI. Cardiac mechano-electric feedback in man: clinical relevance. *Progress in Biophysics and Molecular Biology*. 1999;71:139–154.
7. Peyronnet R, Nerbonne JM, Kohl P. Cardiac Mechano-Gated Ion Channels and Arrhythmias. *Circulation Research* [Internet]. 2016 [cited 2022 Jun 26];118:311–329. Available from: https://www.ahajournals.org/doi/abs/10.1161/circresaha.115.305043
8. Cameron BA, Kai H, Kaihara K, Iribe G, Quinn TA. Ischemia Enhances the Acute Stretch-Induced Increase in Calcium Spark Rate in Ventricular Myocytes. *Frontiers in Physiology* [Internet]. 2020 [cited 2022 Jun 23];11:289. Available from: /pmc/articles/PMC7179564/
9. Zhang YH, Youm JB, Earm YE. Stretch-activated non-selective cation channel: A causal link between mechanical stretch and atrial natriuretic peptide secretion. *Progress in Biophysics and Molecular Biology*. 2008;98:1–9.
10. Salameh A, Dhein S. Effects of mechanical forces and stretch on intercellular gap junction coupling. *Biochimica et Biophysica Acta (BBA) - Biomembranes*. 2013;1828:147–156.
11. Cameron BA, Stoyek MR, Bak JJ, Quinn TA. TRPA1 channels are a source of calcium-driven cardiac mechano-arrhythmogenicity. *bioRxiv* [Internet]. 2020 [cited 2020 Dec 2];2020.10.01.321638. Available from: https://doi.org/10.1101/2020.10.01.321638
12. Caporizzo MA, Prosser BL. The microtubule cytoskeleton in cardiac mechanics and heart failure. *Nature Review Cardiology* [Internet]. 2022 [cited 2022 Jun 21];19:364–378. Available from: www.nature.com/nrcardio

13. Prosser BL, Ward CW. Mechano-Chemo Transduction Tunes the Heartstrings. *Sci Signal* [Internet]. 2014 [cited 2022 Jun 27];7:pe7. Available from: /pmc/articles/PMC4372051/

14. Caporizzo MA, Chen CY, Prosser BL. Cardiac microtubules in health and heart disease. *Experimental Biology and Medicine* [Internet]. 2019 [cited 2022 Mar 18];244:1255. Available from: /pmc/articles/PMC6880149/

15. Robison P, Prosser BL. Microtubule mechanics in the working myocyte. *The Journal of Physiology* [Internet]. 2017 [cited 2022 Jun 27];595:3931. Available from: /pmc/articles/PMC5471505/

16. Chen CY, Caporizzo MA, Bedi K, Vite A, Bogush AI, Robison P, Heffler JG, Salomon AK, Kelly NA, Babu A, Morley MP, Margulies KB, Prosser BL. Suppression of detyrosinated microtubules improves cardiomyocyte function in human heart failure. *Nature Medicine* [Internet]. 2018 [cited 2020 Dec 15];24:1225–1233. Available from: /pmc/articles/PMC6195768/?report=abstract

17. Kerr JP, Robison P, Shi G, Bogush AI, Kempema AM, Hexum JK, Becerra N, Harki DA, Martin SS, Raiteri R, Prosser BL, Ward CW. Detyrosinated microtubules modulate mechanotransduction in heart and skeletal muscle. *Nature Communications 2015 6:1* [Internet]. 2015 [cited 2022 Mar 19];6:1–14. Available from: https://www.nature.com/articles/ncomms9526

18. Iribe G, Ward CW, Camelliti P, Bollensdorff C, Mason F, Burton RAB, Garny A, Morphew MK, Hoenger A, Lederer WJ, Kohl P. Axial Stretch of Rat Single Ventricular Cardiomyocytes Causes an Acute and Transient Increase in Ca2+ Spark Rate. *Circ Res* [Internet]. 2009 [cited 2022 Jun 23];104:787. Available from: /pmc/articles/PMC3522525/

19. Horio T, Murata T, Murata T. The role of dynamic instability in microtubule organization. *Frontiers in Plant Science*. 2014;5:511.

20. Warner EF, Li Y, Li X. Targeting Microtubules for the Treatment of Heart Disease. *Circulation Research* [Internet]. 2022 [cited 2022 Jun 21];130:1723–1741. Available from: https://www.ahajournals.org/doi/abs/10.1161/CIRCRESAHA.122.319808

21. Robison P, Caporizzo MA, Ahmadzadeh H, Bogush AI, Chen CY, Margulies KB, Shenoy VB, Prosser BL. Detyrosinated microtubules buckle and bear load in contracting cardiomyocytes. *Science* [Internet]. 2016 [cited 2022 Mar 17];352:aaf0659. Available from: /pmc/articles/PMC5441927/

22. Sanyal C, Pietsch N, Ramirez Rios S, Peris L, Carrier L, Moutin MJ. The detyrosination/re-tyrosination cycle of tubulin and its role and dysfunction in neurons and cardiomyocytes. *Seminars in Cell & Developmental Biology*. 2021;

23. Prota AE, Magiera MM, Kuijpers M, Bargsten K, Frey D, Wieser M, Jaussi R, Hoogenraad CC, Kammerer RA, Janke C, Steinmetz MO. Structural basis of tubulin tyrosination by tubulin tyrosine ligase. *The Journal of Cell Biology* [Internet]. 2013 [cited 2022 Jun 26];200:259. Available from: /pmc/articles/PMC3563685/

24. Chen CY, Caporizzo MA, Bedi K, Vite A, Bogush AI, Robison P, Heffler JG, Salomon AK, Kelly NA, Babu A, Morley MP, Margulies KB, Prosser BL. Suppression of detyrosinated microtubules improves cardiomyocyte function in human heart failure. *Nat Med* [Internet]. 2018 [cited 2022 Jun 23];24:1225. Available from: /pmc/articles/PMC6195768/

25. Caporizzo MA, Chen CY, Salomon AK, Margulies KB, Prosser BL. Microtubules Provide a Viscoelastic Resistance to Myocyte Motion. *Biophysical Journal* [Internet]. 2018 [cited 2022 Jun 23];115:1796. Available from: /pmc/articles/PMC6224693/

26. Caporizzo MA, Prosser BL. Need for Speed: The Importance of Physiological Strain Rates in Determining Myocardial Stiffness. *Frontiers in Physiology*. 2021;12:1183.

27. Kim D. A mechanosensitive K+ channel in heart cells. Activation by arachidonic acid. *Journal of General Physiology* [Internet]. 1992 [cited 2022 Jun 26];100:1021–1040. Available from: http://rupress.org/jgp/article-pdf/100/6/1021/1185528/1021.pdf

28. Kohl P, Bollensdorff C, Garny A. Effects of mechanosensitive ion channels on ventricular electrophysiology: experimental and theoretical models. *Experimental Physiology* [Internet]. 2006 [cited 2022 Jun 27];91:307–321. Available from: https://onlinelibrary.wiley.com/doi/full/10.1113/expphysiol.2005.031062

29. Riemer TL, Tung L. Stretch-induced excitation and action potential changes of single cardiac cells. *Progress in Biophysics and Molecular Biology*. 2003;82:97–110.

30. Wang Z, Ye D, Ye J, Wang M, Liu J, Jiang H, Xu Y, Zhang J, Chen J, Wan J. The TRPA1 Channel in the Cardiovascular System: Promising Features and Challenges. 2019 [cited 2020 Sep 14];10. Available from: www.frontiersin.org

31. Inoue R, Jian Z, Kawarabayashi Y. Mechanosensitive TRP channels in cardiovascular pathophysiology. *Pharmacology and Therapeutics*. 2009;123:371–385.

32. Brierley SM, Castro J, Harrington AM, Hughes PA, Page AJ, Rychkov GY, Blackshaw LA. TRPA1 contributes to specific mechanically activated currents and sensory neuron mechanical hypersensitivity. *The Journal of Physiology* [Internet]. 2011 [cited 2022 Apr 14];589:3575. Available from: /pmc/articles/PMC3167119/

33. Yue Z, Xie J, Yu AS, Stock J, Du J, Yue L. Role of TRP channels in the cardiovascular system. *American Journal of Physiology - Heart and Circulatory Physiology* [Internet]. 2015 [cited 2022 Jun 27];308:H157. Available from: /pmc/articles/PMC4312948/

34. Smani T, Dionisio N, López JJ, Berna-Erro A, Rosado JA. Cytoskeletal and scaffolding proteins as structural and functional determinants of TRP channels. *Biochimica et Biophysica Acta (BBA) - Biomembranes*. 2014;1838:658–664.

35. Izu LT, Kohl P, Boyden PA, Miura M, Banyasz T, Chiamvimonvat N, Trayanova N, Bers DM, Chen-Izu Y. Mechano-Electric and Mechano-Chemo-Transduction in Cardiomyocytes. *J Physiol* [Internet]. 2020 [cited 2022 Jun 27];598:1285. Available from: /pmc/articles/PMC7127983/

36. Prosser BL, Ward CW, Jonathan Lederer W. X-ROS signalling is enhanced and graded by cyclic cardiomyocyte stretch. *Cardiovascular Research* [Internet]. 2013 [cited 2022 Jun 27];98:307. Available from: /pmc/articles/PMC3633162/

37. Quinn TA, Jin H, Lee P, Kohl P. Mechanically Induced Ectopy via Stretch-Activated Cation-Nonselective Channels Is Caused by Local Tissue Deformation and Results in Ventricular Fibrillation if Triggered on the Repolarization Wave Edge (Commotio Cordis). *Circulation: Arrhythmia and Electrophysiology* [Internet]. 2017 [cited 2022 Jun 28];10:e004777. Available from: /pmc/articles/PMC5555388/

38. Kohl P, Nesbitt AD, Cooper PJ, Lei M. Sudden cardiac death by Commotio cordis: Role of mechano-electric feedback. *Cardiovascular Research* [Internet]. 2001 [cited 2022 Jun 26];50:280–289. Available from: https://academic.oup.com/cardiovascres/article/50/2/280/273914

39. Lee TY, Sung CS, Chu YC, Liou JT, Lui PW. Incidence and risk factors of guidewire-induced arrhythmia during internal jugular venous catheterization: Comparison of marked and plain J-wires. *Journal of Clinical Anesthesia*. 1996;8:348–351.

40. Befeler B. Mechanical Stimulation of the Heart: Its Therapeutic Value in Tachyarrhythmias. *Chest*. 1978;73:832–838.

41. Kusminsky RE. Complications of Central Venous Catheterization. *J Am Coll Surg*. 2007;204:681–696.

42. Levine JH, Guarnieri T, Kadish AH, White RI, Calkins H, Kan JS. Changes in myocardial repolarization in patients undergoing balloon valvuloplasty for congenital pulmonary stenosis: evidence for contraction-excitation feedback in humans. *Circulation* [Internet]. 1988 [cited 2022 Jun 27];77:70–77. Available from: https://www.ahajournals.org/doi/abs/10.1161/01.CIR.77.1.70

43. Sutherland GR. Sudden cardiac death: the pro-arrhythmic interaction of an acute loading with an underlying substrate. *European Heart Journal* [Internet]. 2017 [cited 2022 Jun 27];38:2986–2994. Available from: https://academic.oup.com/eurheartj/article/38/40/2986/2962792

44. Bainbridge FA. The influence of venous filling upon the rate of the heart. *The Journal of Physiology* [Internet]. 1915 [cited 2022 Jun 26];50:65–84. Available from: https://onlinelibrary.wiley.com/doi/full/10.1113/jphysiol.1915.sp001736

45. de Jong AM, Maass AH, Oberdorf-Maass SU, van Veldhuisen DJ, van Gilst WH, van Gelder IC. Mechanisms of atrial structural changes caused by stretch occurring before and during early atrial fibrillation. *Cardiovascular Research* [Internet]. 2011 [cited 2022 Mar 18];89:754–765. Available from: https://academic.oup.com/cardiovascres/article/89/4/754/261018

46. Sato H, Nagai T, Kuppuswamy D, Narishige T, Koide M, Menick DR, IV GC. Microtubule Stabilization in Pressure Overload Cardiac Hypertrophy. *The Journal of Cell Biology* [Internet]. 1997 [cited 2021 Sep 20];139:963. Available from: /pmc/articles/PMC2139973/

47. Caporizzo MA, Chen CY, Bedi K, Margulies KB, Prosser BL. Microtubules increase diastolic stiffness in failing human cardiomyocytes and myocardium. *Circulation* [Internet]. 2020 [cited 2022 Jun 23];141:902. Available from: /pmc/articles/PMC7078018/

48. Imazio M, Nidorf M. Colchicine and the heart. *European Heart Journal* [Internet]. 2021 [cited 2022 Jun 21];42:2745–2760. Available from: https://academic.oup.com/eurheartj/article/42/28/2745/6271392

49. Zhang Y, Qi Y, Li J-J, He W-J, Gao X-H, Zhang Y, Sun X, Tong J, Zhang J, Deng X-L, Du X-J, Xie W. Stretch-induced sarcoplasmic reticulum calcium leak is causatively associated with atrial fibrillation in pressure-overloaded hearts. *Cardiovascular Research* [Internet]. 2020 [cited 2020 Sep 14];Available from: https://academic.oup.com/cardiovascres/advance-article/doi/10.1093/cvr/cvaa163/5856737

50. Ravelli F. Mechano-electric feedback and atrial fibrillation. *Progress in Biophysics and Molecular Biology*. 2003;82:137–149.

51. Düzen I v., Yavuz F, Vuruskan E, Saracoglu E, Poyraz F, Göksülük H, Candemir B, Demiryürek S. Leukocyte TRP channel gene expressions in patients with non-valvular atrial fibrillation. *Scientific Reports 2017 7:1* [Internet]. 2017 [cited 2022 Jun 22];7:1–7. Available from: https://www.nature.com/articles/s41598-017-10039-0

52. Greiner J, Schiatti T, Kaltenbacher W, Dente M, Semenjakin A, Kok T, Fiegle DJ, Seidel T, Ravens U, Kohl P, Peyronnet R, Rog-Zielinska EA. Consecutive-Day Ventricular and Atrial Cardiomyocyte Isolations from the Same Heart: Shifting the Cost–Benefit Balance of Cardiac Primary Cell Research. *Cells* [Internet]. 2022 [cited 2022 Apr 14];11. Available from: /pmc/articles/PMC8773758/

53. Glick MR, Burns AH, Reddy WJ. Dispersion and isolation of beating cells from adult rat heart. *Analytical Biochemistry*. 1974;61:32–42.

54. Berry MN, Friend DS, Scheuer J. Morphology and metabolism of intact muscle cells isolated from adult rat heart. *Circ Res*. 1970;26:679–687.

55. Dani AM, Cittadini A, Flamini G, Festuccia G, Terranova T. Preparation and some properties of isolated beating myocytes from adult rabbit heart. *Journal of Molecular and Cellular Cardiology*. 1977;9:777–784.

56. Louch WE, Sheehan KA, Wolska BM. Methods in cardiomyocyte isolation, culture, and gene transfer. Journal of Molecular and Cellular Cardiology. 2011;51:288–298.

57. Cerbai E, Sartiani L, De Paoli P, Mugelli A. Isolated cardiac cells for electropharmacological studies. *Pharmacological Research*. 2000;42:1–8.

58. Shioya T. A Simple Technique for Isolating Healthy Heart Cells from Mouse Models. *The Journal of Physiological Sciences*. 2007;57:327–335.

59. Voigt N, Pearman CM, Dobrev D, Dibb KM. Methods for isolating atrial cells from large mammals and humans. Journal of Molecular and Cellular Cardiology. 2015;86:187–198.

60. Dipla K, Mattiello JA, Jeevanandam V, Houser SR, Margulies KB. Myocyte recovery after mechanical circulatory support in humans with end-stage heart failure. *Circulation*. 1998;97:2316–2322.

61. Guo G, Chen L, Rao M, Chen K, Song J, Hu S. A modified method for isolation of human cardiomyocytes to model cardiac diseases. *Journal of Translational Medicine* [Internet]. 2018 [cited 2021 Mar 17];16:288. Available from: https://translational-medicine.biomedcentral.com/articles/10.1186/s12967-018-1649-6

62. Zimmerman ANE, Daems W, Hülsmann WC, Snijder J, Wisse E, Durrer D. Morphological Changes of Heart Muscle Caused by Successive Perfusion with Calcium-free and Calcium-containing Solutions (Calcium Paradox). *Cardiovascular Research*. 1967;1:201–209.

63. Piper HM. The calcium paradox revisited: An artefact of great heuristic value. *Cardiovascular Research*. 2000;45:123–127.

64. Zimmerman ANE, Hülsmann WC. Paradoxical Influence of Calcium Ions on the Permeability of the Cell Membranes of the Isolated Rat Heart. *Nature 1966 211:5049*. 1966;211:646–647.

65. Hülsmann WC. Morphological changes of heart muscle caused by successive perfusion with calcium-free and calcium-containing solutions (calcium paradox). *Cardiovascular Research*. 2000;45:122–122.

66. Yates JC, Dhalla NS. Structural and functional changes associated with failure and recovery of hearts after perfusion with Ca2+-free medium. *Journal of Molecular and Cellular Cardiology*. 1975;7:91–103.

67. Daly MJ, Elz JS, Nayler WG. Contracture and the calcium paradox in the rat heart. *Circulation Research*. 1987;61:560–569.

68. Daly MJ, Elz JS, Nayler WG. Contracture and the calcium paradox in the rat heart. *Circulation Research*. 1987;61:560–569.

69. Frank JS, Rich TL, Beydler S, Kreman M. Calcium depletion in rabbit myocardium. Ultrastructure of the sarcolemma and correlation with the calcium paradox. *Circulation Research*. 1982;51:117–130.

70. Rodrigo GC, Chapman RA. The calcium paradox in isolated guinea-pig ventricular myocytes: effects of membrane potential and intracellular sodium. *The Journal of Physiology*. 1991;434:627.

71. Alto LE, Elimban V, Lukas A, Dhalla NS. Modification of heart sarcolemmal Na + /K +-ATPase activity during development of the calcium paradox. *Molecular and Cellular Biochemistry*. 2000;207:87–94.

72. Fuller W, Parmar V, Eaton P, Bell JR, Shattock MJ. Cardiac ischemia causes inhibition of the Na/K ATPase by a labile cytosolic compound whose production is linked to oxidant stress. *Cardiovascular Research* [Internet]. 2003 [cited 2022 Jun 27];57:1044–1051. Available from: https://academic.oup.com/cardiovascres/article/57/4/1044/346621

73. Chatamra KR, Chapman RA. The effects of sodium-calcium exchange inhibitors on protein loss associated with the calcium paradox of the isolated Langendorff perfused guinea-pig heart. *Experimental Physiology*. 1996;81:203–210.

74. Omachi A, Kleps RA, Henderson TO, Labotka RJ. Inhibition of the calcium paradox in isolated rat hearts by high perfusate sucrose concentrations. *https://doi.org/101152/ajpheart19942665H1729*. 1994;266.

75. Watanabe Y, Iwamoto T, Matsuoka I, Ohkubo S, Ono T, Watano T, Shigekawa M, Kimura J. Inhibitory effect of 2,3-butanedione monoxime (BDM) on Na+/Ca2+ exchange current in guinea-pig cardiac ventricular myocytes. *British Journal of Pharmacology*. 2001;132:1317.

76. Mulieri LA, Hasenfuss G, Ittleman F, Blanchard EM, Alpert NR. Protection of human left ventricular myocardium from cutting injury with 2,3-butanedione monoxime. *Circulation Research*. 1989;65:1441–1444.

77. Pinz I, Zhu M, Mende U, Ingwall JS. An Improved Isolation Procedure for Adult Mouse Cardiomyocytes. *Cell Biochemistry and Biophysics*. 2011;61:93–101.

78. Xu YJ, Saini HK, Zhang M, Elimban V, Dhalla NS. MAPK activation and apoptotic alterations in hearts subjected to calcium paradox are attenuated by taurine. *Cardiovascular Research*. 2006;72:163–174.

79. Quinn TA, Kohl P. Rabbit models of cardiac mechano-electric and mechano-mechanical coupling. Progress in Biophysics and Molecular Biology. 2016;121:110–122.

80. Odening KE, Baczko I, Brunner M, Mechanisms KG, de Medeiros RA, Hausen ZA. Animals in cardiovascular research: important role of rabbit models in cardiac electrophysiology. *Br J Pharmacol* [Internet]. 2020 [cited 2022 Apr 16];41:2046–2061. Available from: https://academic.oup.com/eurheartj/article/41/21/2036/5837789

81. Nánási PP, Horváth B, Tar F, Almássy J, Szentandrássy N, Jost N, Baczkó I, Bányász T, Varró A. Canine myocytes represent a good model for human ventricular cells regarding their electrophysiological properties. *Pharmaceuticals*. 2021;14:748.

82. Denyer JC, Brown HF. Rabbit sino-atrial node cells: isolation and electrophysiological properties. *The Journal of Physiology*. 1990;428:405.

83. Jansen HJ, Rose RA. Isolation of Atrial Myocytes from Adult Mice. *JoVE (Journal of Visualized Experiments)*. 2019;2019:e59588.

84. Wright PT, Tsui SF, Francis AJ, MacLeod KT, Marston SB. Approaches to High-Throughput Analysis of Cardiomyocyte Contractility. *Frontiers in Physiology*. 2020;11:612.

85. Tomsits P, Schüttler D, Kääb S, Clauss S, Voigt N. Isolation of high quality murine atrial and ventricular myocytes for simultaneous measurements of Ca2+ transients and l-type calcium current. *Journal of Visualized Experiments*. 2020;2020:1–17.

86. Louch WE, Sheehan KA, Wolska BM. Methods in cardiomyocyte isolation, culture, and gene transfer. Journal of Molecular and Cellular Cardiology. 2011;51:288–298.

87. Santangelo C. Worthington Biochemical Online Tissue Dissociation Guide [Internet]. Worthington Biochemical Corporation. 2011 [cited 2022 Apr 19];Available from: https://www.worthington-biochem.com/tissuedissociation/basic.html

88. Ackers-Johnson M, Li PY, Holmes AP, O'Brien SM, Pavlovic D, Foo RS. A Simplified, Langendorff-Free Method for Concomitant Isolation of Viable Cardiac Myocytes and Nonmyocytes from the Adult Mouse Heart. *Circulation Research*. 2016;119:909–920.

89. MacIanskiene R, Martisiene I, Zablockaite D, Gendviliene V. Characterization of Mg2+-regulated TRPM7-like current in human atrial myocytes. *Journal of Biomedical Science*. 2012;19:75.

90. Isenberg G, Klockner U. Calcium tolerant ventricular myocytes prepared by preincubation in a "KB medium." *Pflügers Archiv 1982 395:1*. 1982;395:6–18.

91. Yue L, Feng J, Li GR, Nattel S. Transient outward and delayed rectifier currents in canine atrium: properties and role of isolation methods. *https://doi.org/101152/ajpheart19962706H2157* [Internet]. 1996 [cited 2022 Jun 4];270. Available from: https://journals.physiology.org/doi/abs/10.1152/ajpheart.1996.270.6.H2157

92. Rajamani S, Anderson CL, Valdivia CR, Eckhardt LL, Foell JD, Robertson GA, Kamp TJ, Makielski JC, Anson BD, January CT. Specific serine proteases selectively damage KCNH2 (hERG1) potassium channels and IKr. *American Journal of Physiology - Heart and Circulatory Physiology* [Internet]. 2006 [cited 2022 May 11];290:1278–1288. Available from: https://journals.physiology.org/doi/full/10.1152/ajpheart.00777.2005

93. Struk A, Szücs G, Kemmer H, Melzer W. Fura-2 calcium signals in skeletal muscle fibres loaded with high concentrations of EGTA. *Cell Calcium*. 1998;23:23–32.

94. Díaz ME, Trafford AW, Eisner DA. The Effects of Exogenous Calcium Buffers on the Systolic Calcium Transient in Rat Ventricular Myocytes. 2001.

95. Cameron BA, Stoyek MR, Bak JJ, Connolly MS, DeLong EA, Greiner J, Peyronnet R, Kohl P, Quinn TA. The cardiac TRPA1 channel drives calcium-mediated mechano-arrhythmogenesis. *bioRxiv*. 2022;2020.10.01.321638.

96. Le Guennec JY, Peineau N, Argibay JA, Mongo KG, Garnier D. A new method of attachment of isolated mammalian ventricular myocytes for tension recording: Length dependence of passive and active tension. *Journal of Molecular and Cellular Cardiology*. 1990;22:1083–1093.

97. Voigt N, Zhou XB, Dobrev D. Isolation of human atrial myocytes for simultaneous measurements of Ca2+ transients and membrane currents. *Journal of Visualized Experiments*. 2013;50235.

98. You Y, Pelzer DJ, Pelzer S. Modulation of L-Type Ca2" Current by Fast and Slow Ca2' Buffering in Guinea Pig Ventricular Cardiomyocytes. *Biophysical Journal*. 1997;72:175–187.

99. Struk A, Szücs G, Kemmer H, Melzer W. Fura-2 calcium signals in skeletal muscle fibres loaded with high concentrations of EGTA. *Cell Calcium*. 1998;23:23–32.

100. Grinwald PM, Nayler WG. Calcium entry in the calcium paradox. *Journal of Molecular and Cellular Cardiology*. 1981;13:867–880.

101. Bustamante JO, Watanabe T, Murphy DA, McDonald TF. Isolation of single atrial and ventricular cells from the human heart. *Canadian Medical Association Journal* [Internet]. 1982 [cited 2022 May 2];126:791. Available from: /pmc/articles/PMC1863102/?report=abstract

102. MacIanskiene R, Martisiene I, Zablockaite D, Gendviliene V. Characterization of Mg2+-regulated TRPM7-like current in human atrial myocytes. *Journal of Biomedical Science*. 2012;19:75.

103. Dobrev D, Wettwer E, Himmel HM, Kortner A, Kuhlisch E, Schüler S, Siffert W, Ravens U. G-Protein β3-Subunit 825T Allele Is Associated With Enhanced Human Atrial Inward Rectifier Potassium Currents. *Circulation*. 2000;102:692–697.

104. Veldkamp MW, Geuzebroek GSC, Baartscheer A, Verkerk AO, Schumacher CA, Suarez GG, Berger WR, Casini S, van Amersfoorth SCM, Scholman KT, Driessen AHG, Belterman CNW, van Ginneken ACG, de Groot JR, de Bakker JMT, Remme CA, Boukens BJ, Coronel R. Neurokinin-3 receptor activation selectively prolongs atrial refractoriness by inhibition of a background K+ channel. *Nature Communications*. 2018;9.

105. Coppini R, Ferrantini C, Aiazzi A, Mazzoni L, Sartiani L, Mugelli A, Poggesi C, Cerbai E. Isolation and Functional Characterization of Human Ventricular Cardiomyocytes from Fresh Surgical Samples. *Journal of Visualized Experiments : JoVE*. 2014;51116.

106. Wolska BM, John Solaro R. Method for isolation of adult mouse cardiac myocytes for studies of contraction and microfluorimetry. *American Journal of Physiology - Heart and Circulatory Physiology*. 1996;271.

107. Ferreira G, Artigas P, Pizarro G, Brum G. Butanedione Monoxime Promotes Voltage-dependent Inactivation ofL-Type Calcium Channels in Heart. Effects on Gating Currents. *Journal of Molecular and Cellular Cardiology*. 1997;29:777–787.

108. Hooke R. Lectures de potentia restitutiva, or, Of spring explaining the power of springing bodies : to which are added some collections viz. a description of Dr. Pappins wind-fountain and force-pump, Mr. Young's observation concerning natural fountains, some other considerations concerning that subject, Captain Sturmy's remarks of a subterraneous cave and cistern, Mr. G.T. observations made on the Pike of Teneriff, 1674, some reflections and conjectures occasioned thereupon, a relation of a late eruption. London: Royal Society; 1678.

109. Iribe G, Helmes M, Kohl P. Force-length relations in isolated intact cardiomyocytes subjected to dynamic changes in mechanical load. *American Journal of Physiology - Heart and Circulatory Physiology*. 2007;292:1487–1497.

110. Peyronnet R, Bollensdorff C, Capel RA, Rog-Zielinska EA, Woods CE, Charo DN, Lookin O, Fajardo G, Ho M, Quertermous T, Ashley EA, Kohl P. Load-dependent effects of apelin on murine cardiomyocytes. *Progress in Biophysics and Molecular Biology*. 2017;130:333.

111. Schiff PB, Fant J, Horwitz SB. Promotion of microtubule assembly in vitro by taxol. *Nature*. 1979;277:665–667.

112. Parker KK, Taylor LK, Atkinson B, Hansen DE, Wikswo JP. The effects of tubulin-binding agents on stretch-induced ventricular arrhythmias. *European Journal of Pharmacology*. 2001;417:131–140.

113. Kerr JP, Robison P, Shi G, Bogush AI, Kempema AM, Hexum JK, Becerra N, Harki DA, Martin SS, Raiteri R, Prosser BL, Ward CW. Detyrosinated microtubules modulate mechanotransduction in heart and skeletal muscle. *Nature Communications 2015 6:1* [Internet]. 2015 [cited 2022 Apr 15];6:1–14. Available from: https://www.nature.com/articles/ncomms9526

114. Robison P, Caporizzo MA, Ahmadzadeh H, Bogush AI, Chen CY, Margulies KB, Shenoy VB, Prosser BL. Detyrosinated microtubules buckle and bear load in contracting cardiomyocytes. *Science* [Internet]. 2016 [cited 2022 Jun 23];352:aaf0659. Available from: /pmc/articles/PMC5441927/

115. McNamara CR, Mandel-Brehm J, Bautista DM, Siemens J, Deranian KL, Zhao M, Hayward NJ, Chong JA, Julius D, Moran MM, Fanger CM. TRPA1 mediates formalin-induced pain. *Proc Natl Acad Sci U S A*. 2007;104:13525.

116. Vilceanu D, Stucky CL. TRPA1 Mediates Mechanical Currents in the Plasma Membrane of Mouse Sensory Neurons. *PLOS ONE*. 2010;5:e12177.

117. Cameron B. Cellular and Subcellular Mechanisms of Ventricular Mechano-Arrhythmogenicity [Internet]. 2021 [cited 2022 Jun 14];Available from: https://dalspace.library.dal.ca//handle/10222/80606

118. Bögeholz N, Pauls P, Dechering DG, Frommeyer G, Goldhaber JI, Pott C, Eckardt L, Müller FU, Schulte JS. Distinct occurrence of proarrhythmic afterdepolarizations in atrial versus ventricular cardiomyocytes: Implications for translational research on atrial arrhythmia. *Frontiers in Pharmacology*. 2018;9:933.

119. Caves RE, Cheng H, Choisy SC, Gadeberg HC, Bryant SM, Hancox JC, James AF. Atrial-ventricular differences in rabbit cardiac voltage-gated Na 1 currents: Basis for atrial-selective block by ranolazine. *Heart Rhythm* [Internet]. 2017 [cited 2022 Jun 21];14:1657–1664. Available from: http://dx.doi.org/10.1016/j.hrthm.2017.06.012

120. Kurhanewicz N, McIntosh-Kastrinsky R, Tong H, Ledbetter A, Walsh L, Farraj A, Hazari M. TRPA1 mediates changes in heart rate variability and cardiac mechanical function in mice exposed to acrolein. *Toxicol Appl Pharmacol* [Internet]. 2017 [cited 2022 Jun 22];324:51. Available from: /pmc/articles/PMC5391294/

121. Cameron BA, Stoyek MR, Bak JJ, Connolly MS, DeLong EA, Greiner J, Peyronnet R, Kohl P, Alexander Quinn T. The cardiac TRPA1 channel drives calcium-mediated mechano-arrhythmogenesis. bioRxiv. 2020;

122. Jakob D, Klesen A, Allegrini B, Darkow E, Aria D, Emig R, Chica AS, Rog-Zielinska EA, Guth T, Beyersdorf F, Kari FA, Proksch S, Hatem SN, Karck M, Künzel SR, Guizouarn H, Schmidt C, Kohl P, Ravens U, Peyronnet R. Piezo1 and BKCa channels in human atrial fibroblasts: Interplay and remodelling in atrial fibrillation. *Journal of Molecular and Cellular Cardiology*. 2021;158:49–62.

123. Henein MY, Holmgren A, Lindqvist P. Left atrial function in volume versus pressure overloaded left atrium. *International Journal of Cardiovascular Imaging* [Internet]. 2015 [cited 2022 Jun 24];31:959–965. Available from: https://link.springer.com/article/10.1007/s10554-015-0638-6

124. Brunner NW, Haddad F, Kobayashi Y, Hsi A, Swiston JR, Gin KG, Zamanian RT. Prognostic Utility of Right Atrial Emptying Fractions in Pulmonary Arterial Hypertension. *Pulmonary Circulation* [Internet]. 2015 [cited 2022 Jun 24];5:473–480. Available from: https://onlinelibrary.wiley.com/doi/full/10.1086/682218

125. Shah T, Manthena P, Patel C, Chuah A, Hardin EA, Torres F, Bartolome SD, Chin KM. Prognostic Value of Echocardiographic Variables Before and After Initiation of Parenteral Prostacyclin Therapy: An Observational Study. *Chest*. 2022;

126. Tagawa H, Wang N, Narishige T, Ingber DE, Zile MR, Cooper IV G. Cytoskeletal Mechanics in Pressure-Overload Cardiac Hypertrophy. *Circulation Research* [Internet]. 1997 [cited 2022 Jun 24];80:281–289. Available from: https://www.ahajournals.org/doi/abs/10.1161/01.RES.80.2.281

127. Sikkel MB, MacLeod KT, Gordon F. Letter by sikkel et al regarding article, late sodium current inhibition reverses electromechanical dysfunction in human hypertrophic cardiomyopathy. *Circulation*. 2013;128.

128. Coppini R, Ferrantini C, Yao L, Fan P, Del Lungo M, Stillitano F, Sartiani L, Tosi B, Suffredini S, Tesi C, Yacoub M, Olivotto I, Belardinelli L, Poggesi C, Cerbai E, Mugelli A. Late sodium current inhibition reverses electromechanical dysfunction in human hypertrophic cardiomyopathy. *Circulation*. 2013;127:575–584.

129. Sikkel MB, Francis DP, Howard J, Gordon F, Rowlands C, Peters NS, Lyon AR, Harding SE, Macleod KT. Hierarchical statistical techniques are necessary to draw reliable conclusions from analysis of isolated cardiomyocyte studies. *Cardiovascular Research*. 2017;113:1743.

130. Lazic SE. The problem of pseudoreplication in neuroscientific studies: is it affecting your analysis? *BMC Neuroscience*. 2010;11:5.

131. Iribe G, Kaneko T, Yamaguchi Y, Naruse K. Load dependency in force–length relations in isolated single cardiomyocytes. *Progress in Biophysics and Molecular Biology*. 2014;115:103–114.

132. Virk HS, Rekas MZ, Biddle MS, Wright AKA, Sousa J, Weston CA, Chachi L, Roach KM, Bradding P. Validation of antibodies for the specific detection of human TRPA1. *Scientific Reports*. 2019;9.

133. Vetter I, Touska F, Hess A, Hinsbey R, Sattler S, Lampert A, Sergejeva M, Sharov A, Collins LS, Eberhardt M, Engel M, Cabot PJ, Wood JN, Vlachová V, Reeh PW, Lewis RJ, Zimmermann K. Ciguatoxins activate specific cold pain pathways to elicit burning pain from cooling. *The EMBO Journal*. 2012;31:3795.

134. Yu S, Gao G, Peterson BZ, Ouyang A. TRPA1 in mast cell activation-induced long-lasting mechanical hypersensitivity of vagal afferent C-fibers in guinea pig esophagus. *American Journal of Physiology - Gastrointestinal and Liver Physiology*. 2009;297:34–42.

135. Mitchell EJ, Ahmed K, Breeman S, Cotton S, Constable L, Ferry G, Goodman K, Hickey H, Meakin G, Mironov K, Quann N, Wakefield N, McDonald A. It is unprecedented: Trial management during the COVID-19 pandemic and beyond. *Trials* [Internet]. 2020 [cited 2022 Jun 24];21:1–7. Available from: https://trialsjournal.biomedcentral.com/articles/10.1186/s13063-020-04711-6

136. Taylor AH, Mitchell AE, Mitchell IM. A 15-year study of the changing demographics and infection risk in a new UK cardiac surgery unit. *Interactive Cardiovascular and Thoracic Surgery*. 2012;15:390.

137. Pierri MD, Capestro F, Zingaro C, Torracca L. The changing face of cardiac surgery patients: an insight into a Mediterranean region. *European Journal of Cardio-Thoracic Surgery*. 2010;38:407–413.

138. Wojnilowicz M, Besford QA, Wu YL, Loh XJ, Braunger JA, Glab A, Cortez-Jugo C, Caruso F, Cavalieri F. Glycogen-nucleic acid constructs for gene silencing in multicellular tumor spheroids. *Biomaterials*. 2018;176:34–49.

139. Schotten U, De Haan S, Verheule S, Harks EGA, Frechen D, Bodewig E, Greiser M, Ram R, Maessen J, Kelm M, Allessie M, Van Wagoner DR. Blockade of atrial-specific K +-currents increases atrial but not ventricular contractility by enhancing reverse mode Na + /Ca 2+-exchange. *Cardiovascular Research*. 2007;73:37–47.